CHAPTER 6
THE DYNAMIC RESPONSE OF A FREEZE-LINING TO STEP CHANGES IN INPUT HEAT FLOW RATE

This chapter describes a series of experiments conducted with the FLC model. The purpose of these experiments was to study the influence of step changes in input heat flow rate on the dynamic behaviour of the furnace wall and freeze lining. The following aspects were considered:

- Freeze lining thickness.
- Temperature distribution through the furnace wall and freeze lining.
- Time lag in temperature response of the refractory brick wall relative to the time when conditions were changed in the slag bath.
- Liquid slag temperature.
- Composition distribution through the freeze lining.
- Liquid slag composition.

6.1 EXPERIMENTAL SETUP

The model flow diagram used for all experiments in this chapter is shown in Figure 18 (page 49). The geometry and dimensions used are all the same as those given in paragraph 3.6.4a (page 43) except for the layer dimension of the freeze lining layer. This dimension was adjusting according to the nature of each experiment. For experiments where much solidification occurred, a layer thickness of 1.0 to 2.0 m was used. For most of the experiments, however, a thickness of 0.2 m was adequate.

The initial mass of slag used was around 11 ton solid and 230 ton liquid for those cases where a thicker initial freeze lining was used and about 7 ton solid and 234 ton liquid for cases started with a thinner freeze lining. No slag was added or removed from the system during the experiments.

The initial liquid slag composition of all experiments was chosen as 15%-55%-30% (FeO-TiO_2-Ti_2O_3 mass percentages) and the effective thermal conductivity of the liquid slag as 0.005 kW/(m.°C). The liquid slag composition used is located between the eutectic groove and the stoichiometric M_3O_5 line. The average composition of slag in the furnace (solid together with liquid) will differ from this composition due to the difference in composition between the liquid slag and both the pseudobrookite and rutile freeze linings used.

All experiments were run for a period of 24 hours, or until the freeze lining had been melted away completely.

6.2 EXPERIMENTS

The parameters that were varied over the series of experiments include the following:

- Initial steady state heat flow rate.
- Initial freeze lining composition.
- Net input heat flow rate.

The initial steady state heat flow rate fixed the initial temperature distribution in the freeze lining and furnace wall, and the initial freeze lining thickness. The net input heat flow rate was achieved by setting the heat flow rate of the ElectricalPower energy input module and of the HeatLosses energy output module shown in Figure 18 (page 49). The HeatLosses heat flow represented all heat losses from the slag bath other than through the sidewalls and freeze lining in contact with the slag bath. The set of experiments with the various parameters of interest to each experiment are listed in Table 21 below. The set of 26 experiments consists of 3 subsets.

The first subset consists of experiments 6.1 to 6.14. The aim of this set was to test the influence of the net input heat flow rate into the slag bath. Seven experiments were conducted with a net input heat flow rate less than the initial steady state heat flow rate of 250 kW, and seven experiments with a net input heat flow rate greater than the initial steady state heat flow rate. No other parameters were changed. In all cases the freeze lining was filled with solid slag consisting of only pseudobrookite and no rutile. The composition of the pseudobrookite was 37.6% $FeTi_2O_5$ and 62.4% Ti_3O_5 (mass basis). This is the composition of the first solid slag to form from liquid slag with the composition of 15%–55%–30% (FeO–TiO_2–Ti_2O_3 mass percentages) used for all the experiments in this chapter.

The second subset includes experiments 6.15 to 6.20. These experiments were aimed at testing once again the influence of net input heat flow rate, but this time with a different initial steady state heat flow rate (and consequently a different initial freeze lining thickness). Three experiments were conducted with a net input heat flow rate less than the initial steady state heat flow rate of 300 kW, and three experiments with a net input heat flow rate greater than the initial steady state heat flow rate. The freeze lining composition used was the same as for experiments 6.1 to 6.14.

The third subset includes experiments 6.21 to 6.26. The same initial conditions as the first subset were used, except for the composition of the freeze lining. The pseudobrookite solid solution used in the first two subsets was replaced with 100% rutile (TiO_2). The aim of these experiments was to test the influence of the freeze lining composition on the slag bath composition, and to test the influence of net input heat flow rate.

EXPERIMENT NO.	INITIAL STEADY STATE HEAT FLOW	INITIAL FREEZE LINING THICKNESS	INITIAL FREEZE LINING COMPOSITION	ELECTRICAL POWER HEAT FLOW	HEAT LOSSES HEAT FLOW	NET INPUT HEAT FLOW
6.1	250 kW	0.102 m	Pseudobrookite	0 kW	1000 kW	−1000 kW
6.2	250 kW	0.102 m	Pseudobrookite	0 kW	500 kW	−500 kW
6.3	250 kW	0.102 m	Pseudobrookite	0 kW	200 kW	−200 kW
6.4	250 kW	0.102 m	Pseudobrookite	0 kW	100 kW	−100 kW
6.5	250 kW	0.102 m	Pseudobrookite	0 kW	0 kW	0 kW
6.6	250 kW	0.102 m	Pseudobrookite	100 kW	0 kW	100 kW
6.7	250 kW	0.102 m	Pseudobrookite	200 kW	0 kW	200 kW
6.8	250 kW	0.102 m	Pseudobrookite	300 kW	0 kW	300 kW
6.9	250 kW	0.102 m	Pseudobrookite	400 kW	0 kW	400 kW
6.10	250 kW	0.102 m	Pseudobrookite	500 kW	0 kW	500 kW
6.11	250 kW	0.102 m	Pseudobrookite	1000 kW	0 kW	1000 kW
6.12	250 kW	0.102 m	Pseudobrookite	2000 kW	0 kW	2000 kW
6.13	250 kW	0.102 m	Pseudobrookite	5000 kW	0 kW	5000 kW
6.14	250 kW	0.102 m	Pseudobrookite	10000 kW	0 kW	10000 kW
6.15	300 kW	0.066 m	Pseudobrookite	0 kW	1000 kW	−1000 kW
6.16	300 kW	0.066 m	Pseudobrookite	0 kW	0 kW	0 kW

EXPERIMENT NO.	INITIAL STEADY STATE HEAT FLOW	INITIAL FREEZE LINING THICKNESS	INITIAL FREEZE LINING COMPOSITION	ELECTRICAL POWER HEAT FLOW	HEAT LOSSES HEAT FLOW	NET INPUT HEAT FLOW
6.17	300 kW	0.066 m	Pseudobrookite	200 kW	0 kW	200 kW
6.18	300 kW	0.066 m	Pseudobrookite	400 kW	0 kW	400 kW
6.19	300 kW	0.066 m	Pseudobrookite	1000 kW	0 kW	1000 kW
6.20	300 kW	0.066 m	Pseudobrookite	10000 kW	0 kW	10000 kW
6.21	250 kW	0.102 m	Rutile	0 kW	1000 kW	-1000 kW
6.22	250 kW	0.102 m	Rutile	0 kW	0 kW	0 kW
6.23	250 kW	0.102 m	Rutile	200 kW	0 kW	200 kW
6.24	250 kW	0.102 m	Rutile	400 kW	0 kW	400 kW
6.25	250 kW	0.102 m	Rutile	1000 kW	0 kW	1000 kW
6.26	250 kW	0.102 m	Rutile	10000 kW	0 kW	10000 kW

Table 21 – List of experiments conducted for CHAPTER 6.

6.3 EXPERIMENTAL RESULTS

The results from each experiment are presented below using a series of graphs marked from (a) to (h). The set of graphs is presented consistently for all experiments in this chapter. For this reason each graph type in the set is explained below. A discussion of the experimental results follows after the graphical presentation of the results of all experiments conducted as part of this chapter.

(a) Freeze Lining Thickness and Isotherm Graph

This graph contains two sets of lines. The first set is the thick lines indicating the boundaries of the various layers. From bottom to top, these thick lines represent the outer surface of the steel shell (at a radial position of -0.575 m), the interface between the steel shell and the ramming layer (at -0.550 m), the interface between the ramming layer and the brick layer (at -0.500 m), the interface between the brick layer and the freeze lining (at 0.000 m), and the interface between the freeze lining and the liquid slag. Only the last of these lines varies as a function of time as the freeze lining becomes thinner or thicker depending on the scenario.

The second set of lines is drawn thinner and represents isotherms as a function of time and position in the furnace wall or freeze lining. The first isotherm is drawn at a temperature of 100 °C and is found towards the bottom of the graph near the cold steel shell. This curve is followed by more isotherms at intervals of 100 °C towards the top of the graph.

The vertical axis indicates the radial position of layer interfaces and isotherms. The reference point used on this axis is the interface between the brick layer and solid slag. This position is referred to as the hot face of the refractory brick. A positive deviation from this reference point moves towards the centre of the furnace. This axis configuration was chosen to facilitate reading of freeze lining thickness and of isotherm position relative to the refractory hot face.

(b) Liquid Slag Temperature Graph

This graph shows the variation of the liquid slag bath temperature as a function of time. Since the liquid slag temperature cannot vary independently from melting and solidification at the freeze lining, the temperature plotted on this graph provides an indication of the liquidus temperature of the slag.

(c) Temperature Response Time Delay Graph

This graphs aims to show the influence of thermal inertia of the freeze lining and refractory brick on temperature measurements made in the refractory brick.

The horizontal axis indicates the distance from the refractory hot face at which a hypothetical thermocouple is installed. The vertical axis indicates the lag from the time when a change is enforced on the inside of the furnace to when that change is detected by the thermocouple as a temperature change of specified magnitude.

For example, the results of experiment 6.1 (Figure 60, page 144) indicate that a thermocouple installed 0.4 m from the hot face will take just over 4 hours to detect a 1.0 °C change that resulted from the changes enforced on the inside of the furnace. The same thermocouple will take 5.5 hours to detect a 2.5 °C change, 6.75 hours to detect a 5.0 °C change, and 9 hours to detect a 10.0 °C change. This is in strong contrast with a thermocouple installed 0.1 m away from the hot face. Such a thermocouple detects a 1.0 °C change after 1.75 hours, a 2.5 °C change after 2.25 hours, a 5.0 °C change after 2.75 hours and a 10.0 °C after 3.5 hours.

(d) Liquid Slag Composition Graph

This graph shows the mass fractions of the three liquid slag phase constituents (FeO, TiO_2 and Ti_2O_3) as functions of time. Only a single thin solid line is shown for FeO. This line indicates the calculated mass fraction of FeO in the liquid slag as a function of time. Similarly, the thin solid lines for TiO_2 and Ti_2O_3 indicate the calculated mass fraction of these phase constituents as functions of time. The thick solid lines shown for TiO_2 and Ti_2O_3 indicate the eutectic groove composition for these constituents with the calculated mass fraction of FeO as reference.

This graph can for example be interpreted as follows. The results of experiment 6.1 (Figure 60, page 144) indicate that the liquid slag initially contains less TiO_2 and more Ti_2O_3 than the eutectic composition. However, due to solidification and the resulting change in liquid slag composition, the liquid slag reaches the eutectic composition after about 10.25 hours.

(e) Solid Slag Composition Graph

This graph shows the composition of the freeze lining at the interface between the freeze lining and liquid slag as a function of freeze lining thickness. An additional horizontal axis is shown at the top of the graph. This axis indicates time in hours from the start of the experiment. Because the freeze lining thickness does not vary linearly with time, this second axis is not linear. It is only used to provide an indication of the time at which the slag solidified on the surface of the freeze lining. The tick marks on this axis are always 2 hours apart.

The composition of the solid slag is presented by showing both the distribution of mass between phases (rutile and pseudobrookite), and by showing the distribution of mass between constituents of a specific phase. The phases are separated by a thick solid line, and the constituents within a phase are separated by a thin solid line. The rutile phase is always plotted in the lower part of the graph, and pseudobrookite above it.

Refer to the results of experiment 6.1 (Figure 60, page 144) once again as an example. The freeze lining was initialised with only pseudobrookite having a composition of roughly 38%-62% ($FeTiO_5$-Ti_3O_5). As time progressed, the slag solidifying on the surface of the freeze lining became more and more enriched in $FeTi_2O_5$. After about 10.25 hours (the time when the liquid slag reached the eutectic composition), rutile started to solidify as part of the solid slag. The rutile phase consisted of mostly TiO_2 and only a small amount of Ti_2O_3.

This graph is only included in the result set of experiments that showed an increase in freeze lining thickness. The time axis at the top of this graph is only useful for experiments in which only an increase in freeze lining thickness occurred. The arrow in graph (a) indicates the point in time to which the data in graph (e) belongs.

(f) Liquid Slag Composition Ternary Graph

This graph shows four series. The first is a broken line connecting the Ti_3O_5 and $FeTi_2O_5$ (or M_3O_5) compositions. Second is the upper thin solid line that indicates the composition location of the eutectic groove. Thirdly is the lower thin solid line that traces the composition below which (on the ternary graph) iron metal is a stable phase. Finally, the thick solid line shows the compositional variation of the liquid slag. The starting composition of the liquid slag is marked with a circle.

This graph is only shown for experiments during which a significant change in liquid slag composition took place. For most experiments this was not the case, and the variation would have been difficult to view on this type of graph.

(g) Energy Balance Error Graph

This graph shows the energy balance error of the model as a function of time. It is always included as part of the result set to serve as a confirmation of the numerical integrity of the model in addition to the validation experiments that had been done. The energy balance error calculation is outlined below.

The law of energy conservation states that the difference between the enthalpy that has entered the system and the enthalpy that has exited the system is the enthalpy content of the system. All the terms mentioned are calculated relative to the same reference point in time. In the case of the experiments in this chapter, this reference point is always a time zero (00:00:00). In equation form it can be written as:

$$H_{input} - H_{output} = H_{content}$$

In the case of the numerical solution of the model this equation does not hold absolutely since round-off errors and possibly model errors may occur. For this reason, the balance equation can be rewritten as the following error equation.

$$H_{error} = \left(H_{input} - H_{output}\right) - H_{content}$$

The details of the three right-hand-side enthalpy terms can be written based on the model flow sheet shown in Figure 18.

The only enthalpy input is through the ElectricalPower energy input module. The power input of this module is integrated to obtain an enthalpy figure. The balance reference point of time zero is set after the initial mass of slag is added to the MetalBath mixer via the SlagFeed material input module. For this reason no enthalpy from this input is used in the balance.

$$H_{input} = H_{ElectricalPower}$$

Energy exits from the system via the HeatLosses energy output module, and as losses through the FurnaceWall conductor module. The power figures of both these modules are integrated to obtain enthalpy figures.

$$H_{output} = H_{HeatLosses} + H_{FurnaceWall}$$

The enthalpy content of the system is calculated as the sum of the enthalpy contained in the IsoMod1 isothermal module (this includes the content of the MetalBath and MetalBath mixers), and the enthalpy of each of the four layers (steel, ramming, brick and freeze lining) of the FurnaceWall conductor module.

$$H_{content} = H_{IsoMod1} + H_{FurnaceWall,SteelLayer} + H_{FurnaceWall,RammingLayer} + H_{FurnaceWall,BrickLayer} + H_{FurnaceWall,FreezeLining}$$

The typical change in enthalpy content of the IsoMod1 isothermal module over the period of 24 hours modelled during the experiments conducted is 29,000 kWh. When comparing a typical energy balance error of less than 1.0 kWh with this figure it becomes clear that the errors are negligible.

(h) Mass Balance Error Graph

This graph shows the mass balance error of the model as a function of time for the same purpose as graph (g).

The same approach that was used for the energy balance error was used for calculating the mass balance error. Time zero (00:00:00) was also used as reference point. The following mass balance and error equations were used:

$$m_{input} - m_{output} = m_{content}$$

$$m_{error} = \left(m_{input} - m_{output}\right) - m_{content}$$

Figure 18 was once again used as basis for the right-hand-side terms. Because no material entered or exited the system within the 24 hours covered by the experiment, both the input and output terms in the equations can be omitted. The only term that remains is the content term, which was calculated as the sum of the mass of the slag bath, metal bath and the mass of solid slag in the freeze lining layer of the FurnaceWall conductor module. The other three layers of the conductor were not

included in the calculations because the masses of these layers remained constant during the experiments. The right-hand-side terms are detailed as follows:

$$m_{input} = 0$$

$$m_{output} = 0$$

$$m_{content} = m_{SlagBath} + m_{MetalBath} + m_{FurnaceWall,FreezeLining,SolidSlag}$$

The typical total slag mass (both liquid and solid) in the system was around 241 ton. Typical mass balance errors of less than 1 kg that were recorded during experiments can again be seen as negligible.

6.3.1 Experiment 6.1

INITIAL STEADY STATE HEAT FLOW	INITIAL FREEZE LINING THICKNESS	INITIAL FREEZE LINING COMPOSITION	ELECTRICAL POWER HEAT FLOW	HEAT LOSSES HEAT FLOW	NET INPUT HEAT FLOW
250 kW	0.102 m	Pseudobrookite	0 kW	1000 kW	-1000 kW

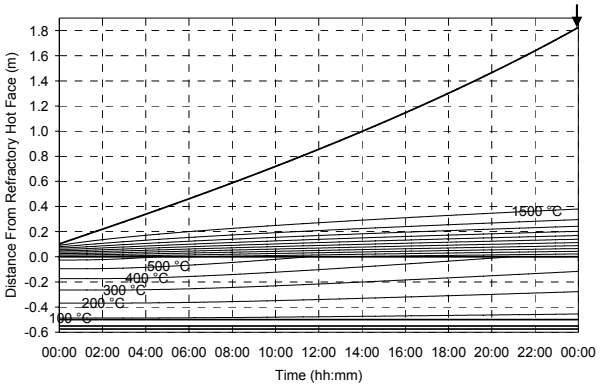

(a)

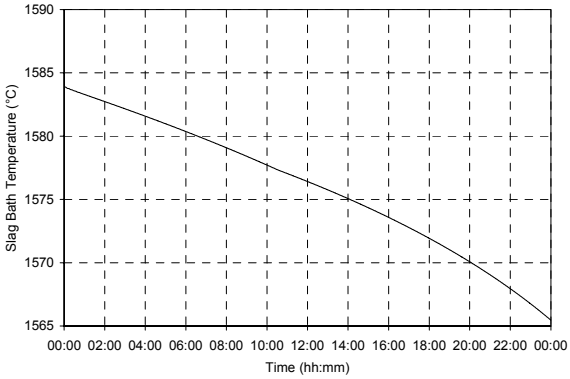

(b)

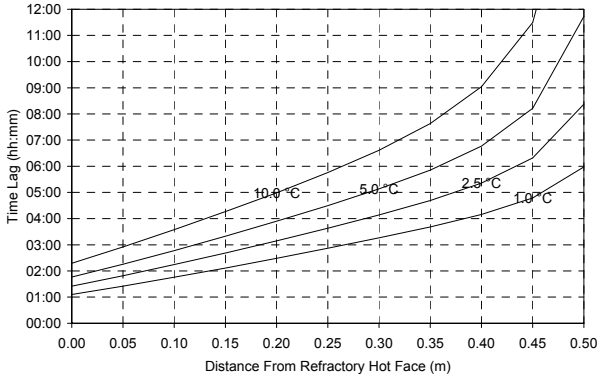

(c)

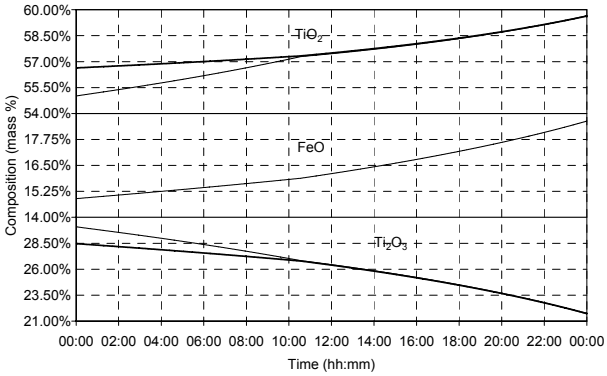

(d)

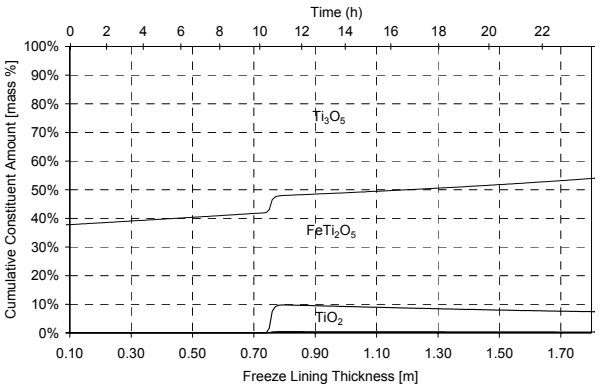

(e)

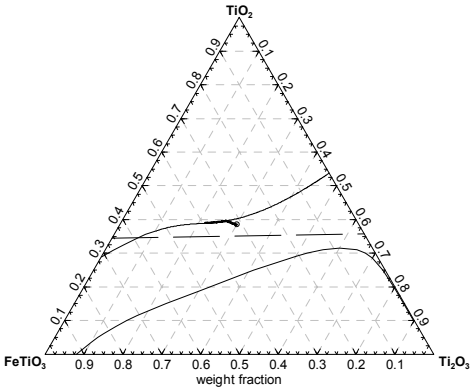

(f)

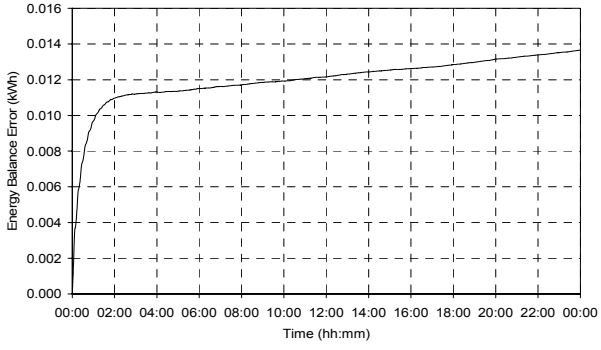

(g)

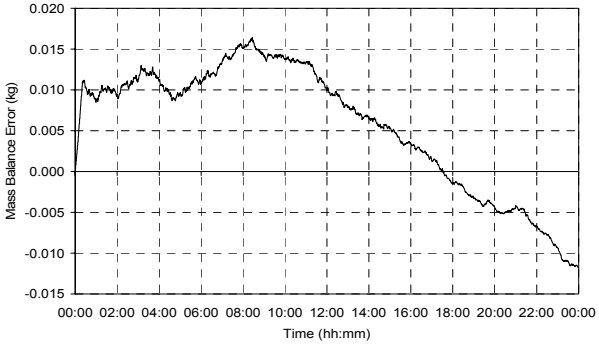

(h)

Figure 60 – Experiment 6.1 results.

6.3.2 Experiment 6.2

INITIAL STEADY STATE HEAT FLOW	INITIAL FREEZE LINING THICKNESS	INITIAL FREEZE LINING COMPOSITION	ELECTRICAL POWER HEAT FLOW	HEAT LOSSES HEAT FLOW	NET INPUT HEAT FLOW
250 kW	0.102 m	Pseudobrookite	0 kW	500 kW	-500 kW

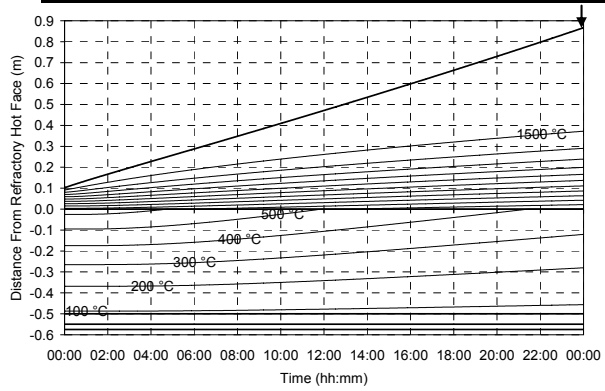

(a)

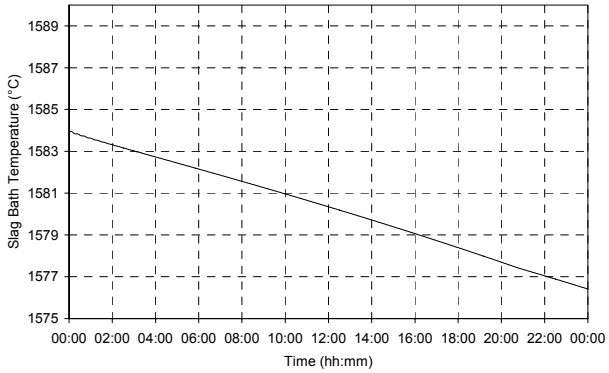

(b)

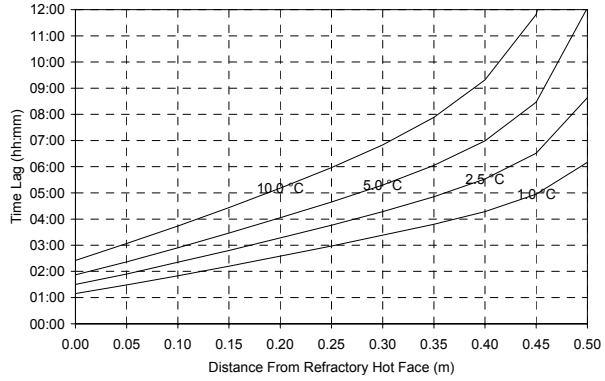

(c)

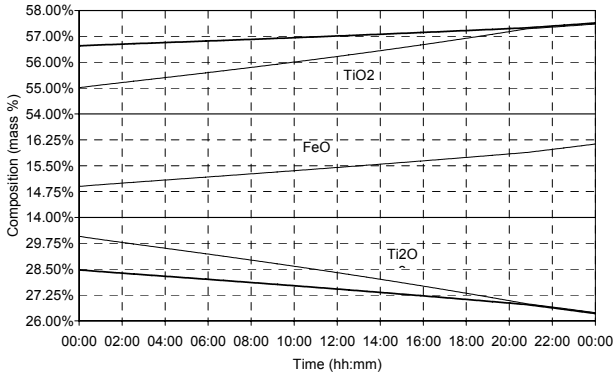

(d)

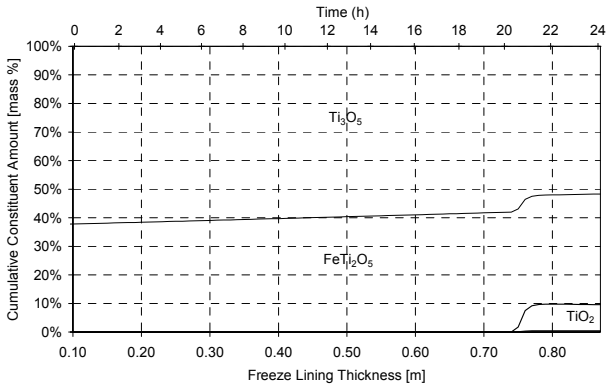

(e)

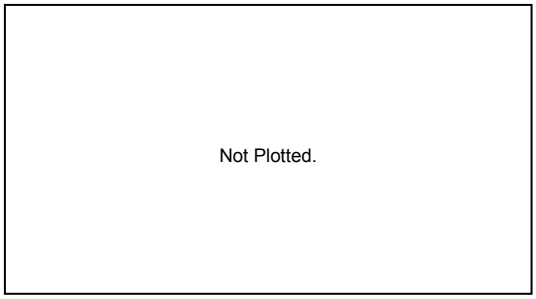

(f)

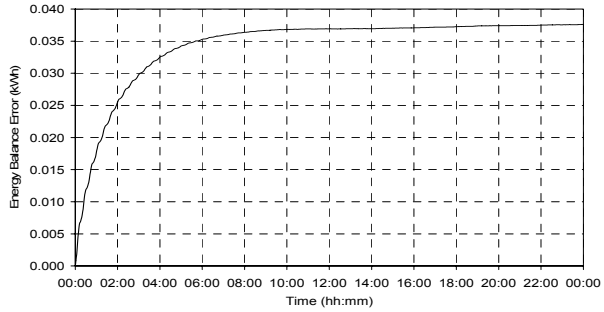

(g)

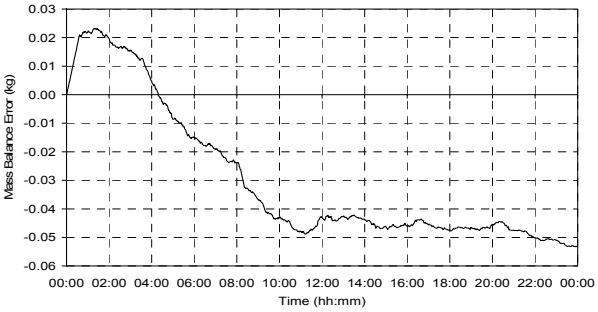

(h)

Figure 61 – Experiment 6.2 results.

6.3.3 Experiment 6.3

INITIAL STEADY STATE HEAT FLOW	INITIAL FREEZE LINING THICKNESS	INITIAL FREEZE LINING COMPOSITION	ELECTRICAL POWER HEAT FLOW	HEAT LOSSES HEAT FLOW	NET INPUT HEAT FLOW
250 kW	0.102 m	Pseudobrookite	0 kW	200 kW	-200 kW

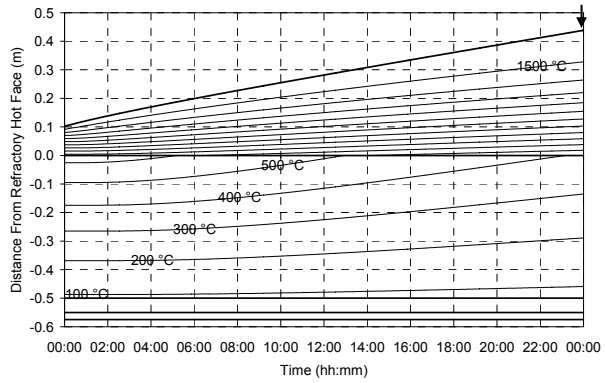

(a)

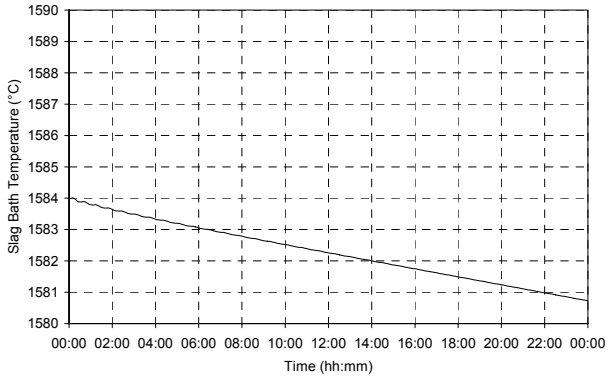

(b)

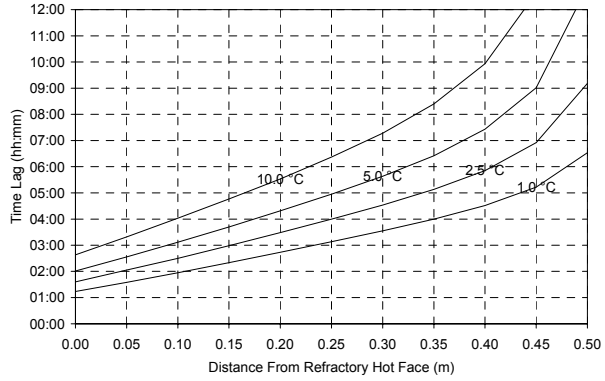

(c)

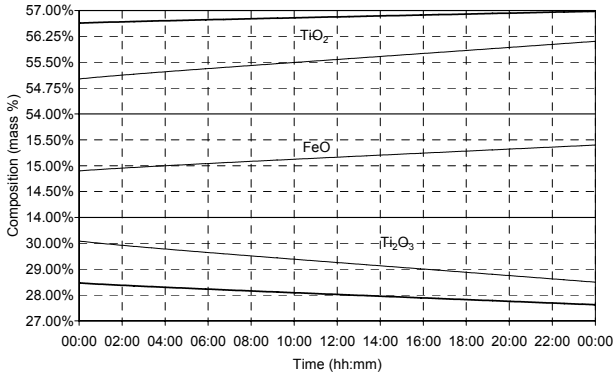

(d)

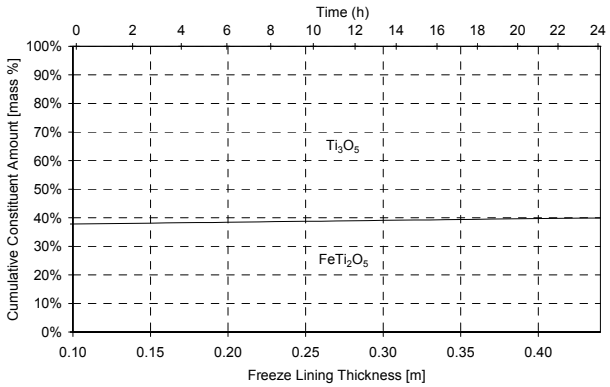

(e)

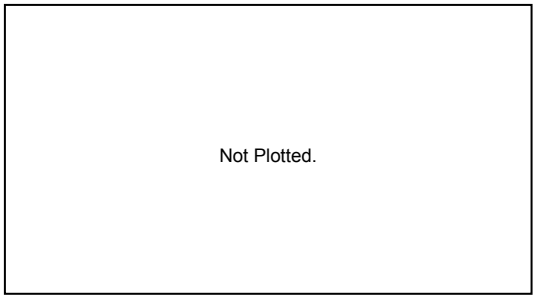

(f)

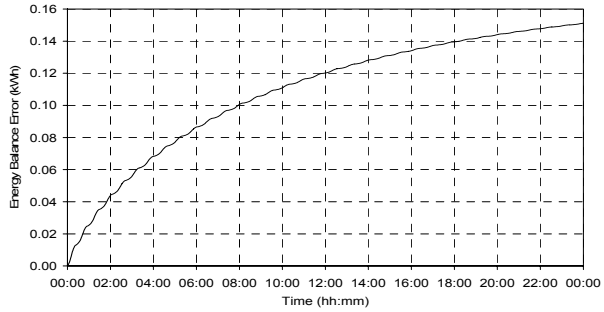

(g)

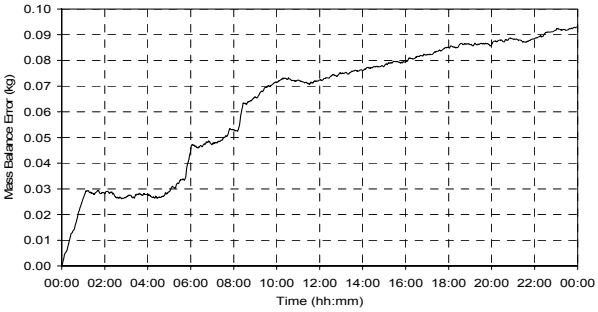

(h)

Figure 62 – Experiment 6.3 results.

6.3.4 Experiment 6.4

INITIAL STEADY STATE HEAT FLOW	INITIAL FREEZE LINING THICKNESS	INITIAL FREEZE LINING COMPOSITION	ELECTRICAL POWER HEAT FLOW	HEAT LOSSES HEAT FLOW	NET INPUT HEAT FLOW
250 kW	0.102 m	Pseudobrookite	0 kW	100 kW	-100 kW

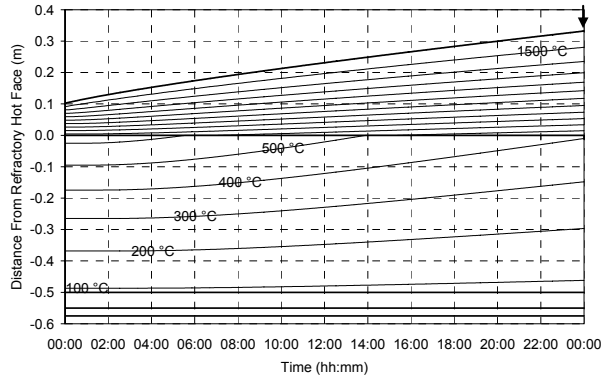

(a)

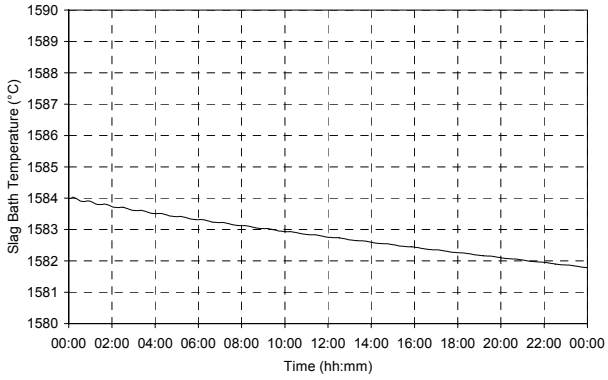

(b)

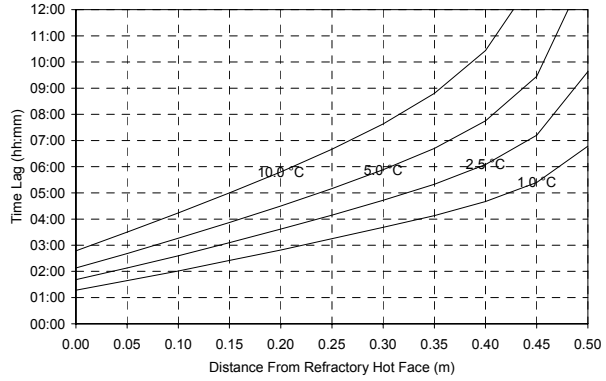

(c)

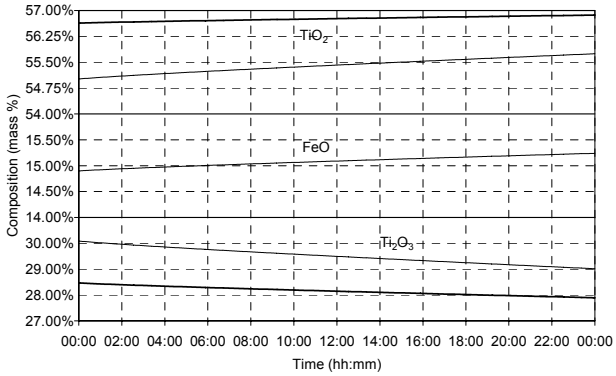

(d)

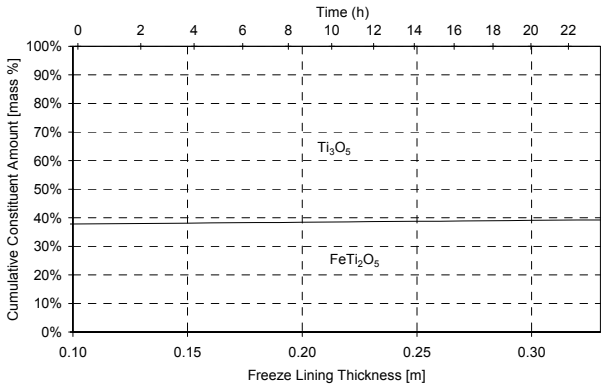

(e)

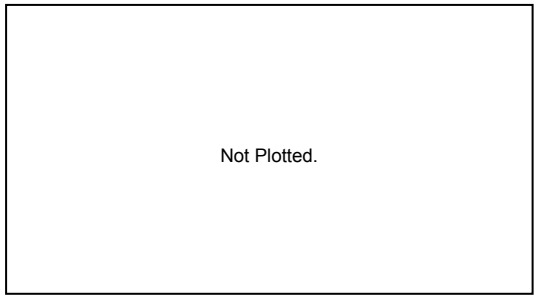

(f)

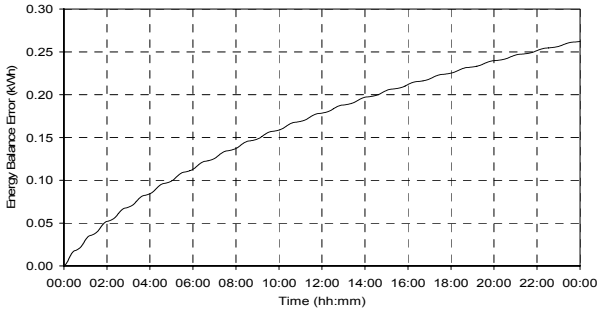

(g)

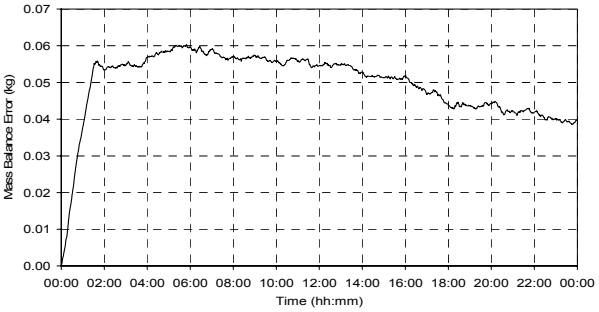

(h)

Figure 63 – Experiment 6.4 results.

6.3.5 Experiment 6.5

INITIAL STEADY STATE HEAT FLOW	INITIAL FREEZE LINING THICKNESS	INITIAL FREEZE LINING COMPOSITION	ELECTRICAL POWER HEAT FLOW	HEAT LOSSES HEAT FLOW	NET INPUT HEAT FLOW
250 kW	0.102 m	Pseudobrookite	0 kW	0 kW	0 kW

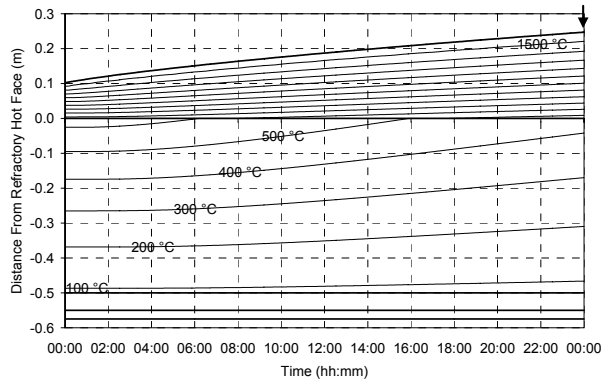

(a)

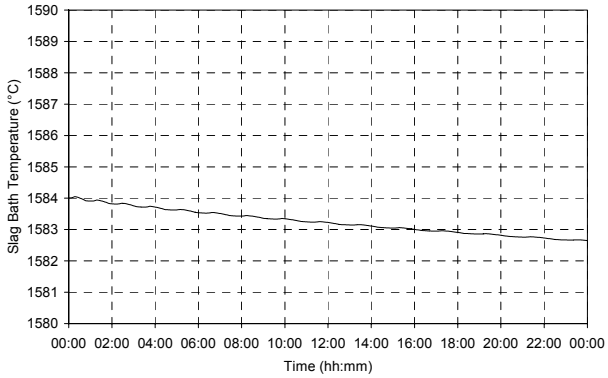

(b)

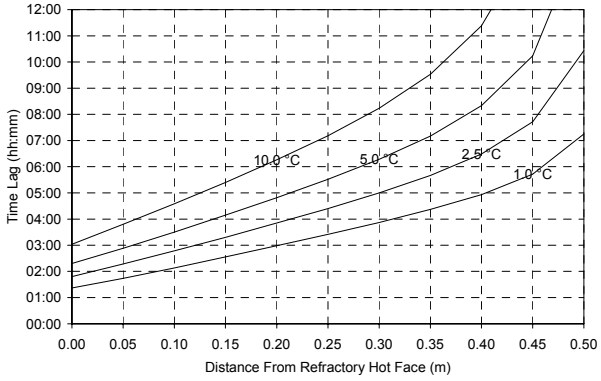

(c)

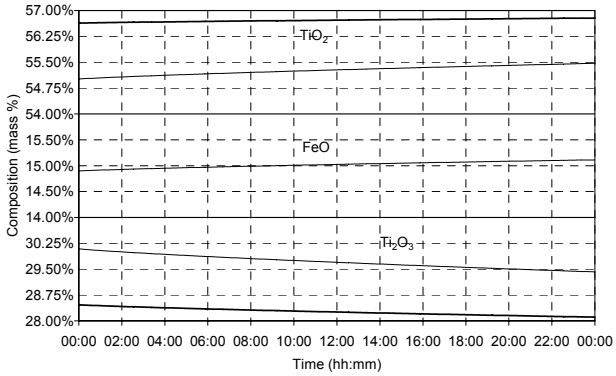

(d)

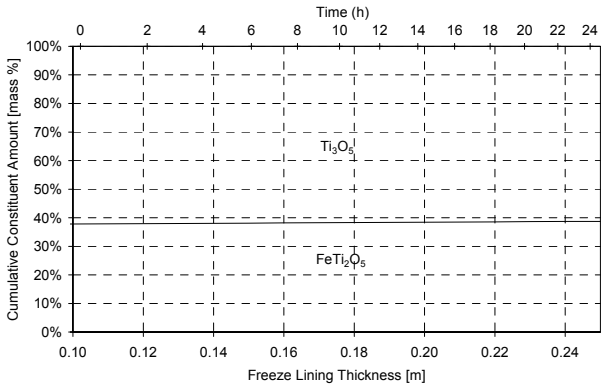

(e)

Not Plotted.

(f)

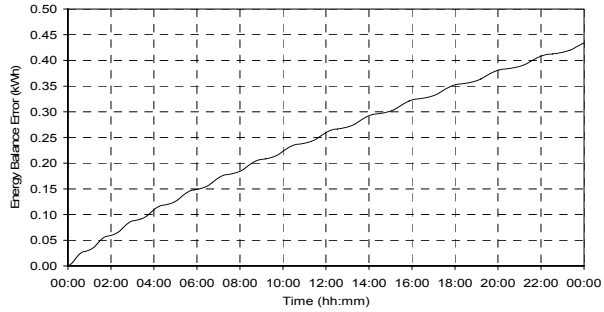

(g)

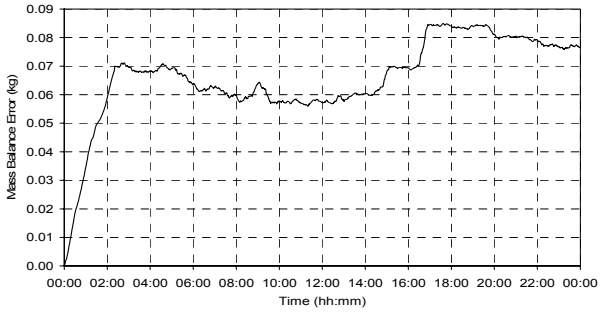

(h)

Figure 64 – Experiment 6.5 results.

6.3.6 Experiment 6.6

INITIAL STEADY STATE HEAT FLOW	INITIAL FREEZE LINING THICKNESS	INITIAL FREEZE LINING COMPOSITION	ELECTRICAL POWER HEAT FLOW	HEAT LOSSES HEAT FLOW	NET INPUT HEAT FLOW
250 kW	0.102 m	Pseudobrookite	100 kW	0 kW	100 kW

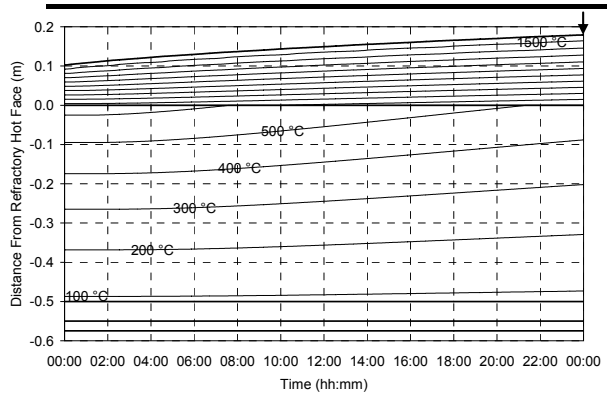

(a)

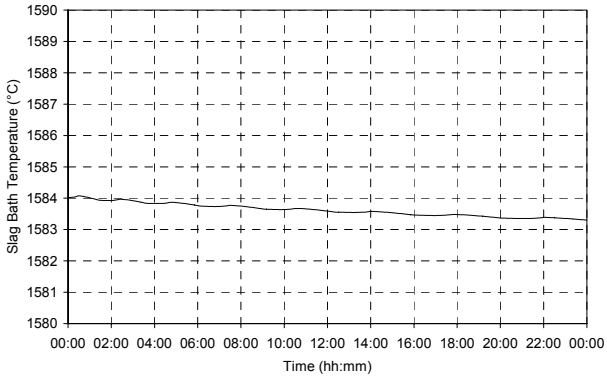

(b)

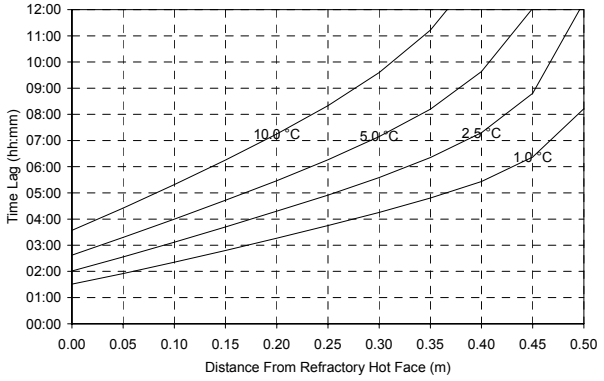

(c)

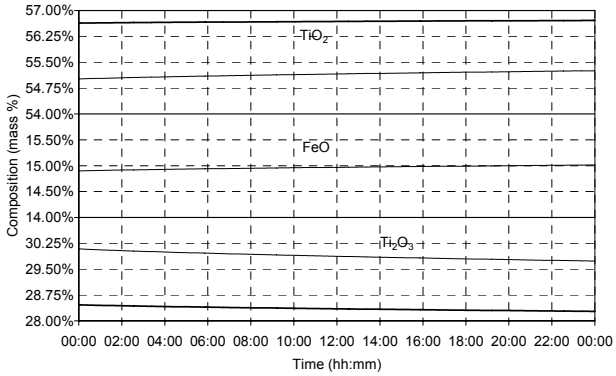

(d)

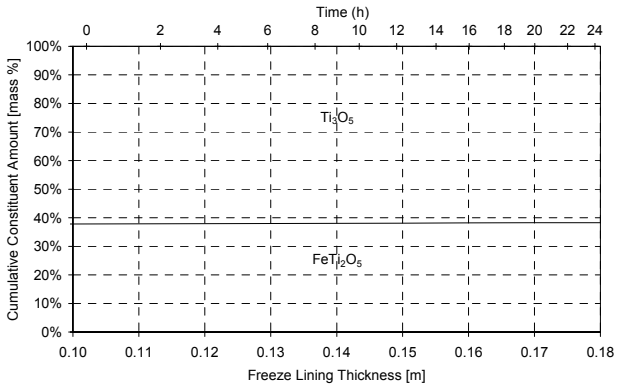

(e)

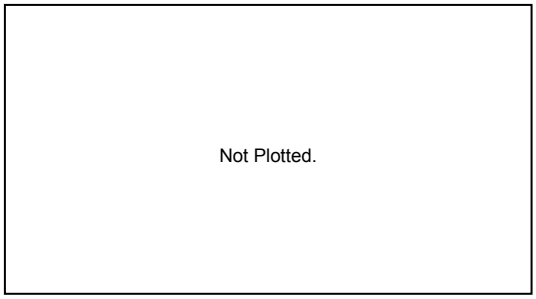

(f)

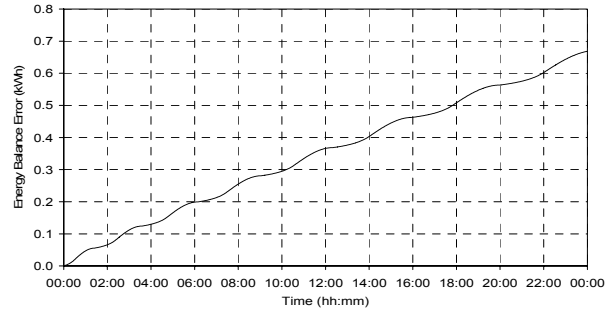

(g)

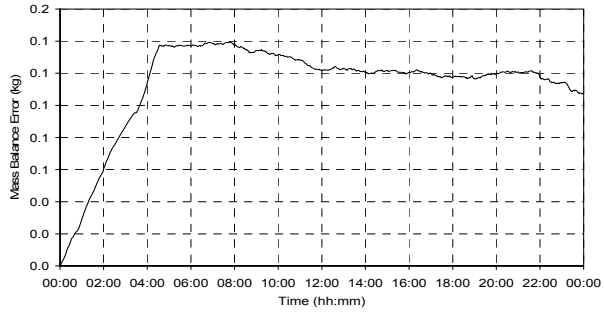

(h)

Figure 65 – Experiment 6.6 results.

6.3.7 Experiment 6.7

INITIAL STEADY STATE HEAT FLOW	INITIAL FREEZE LINING THICKNESS	INITIAL FREEZE LINING COMPOSITION	ELECTRICAL POWER HEAT FLOW	HEAT LOSSES HEAT FLOW	NET INPUT HEAT FLOW
250 kW	0.102 m	Pseudobrookite	200 kW	0 kW	200 kW

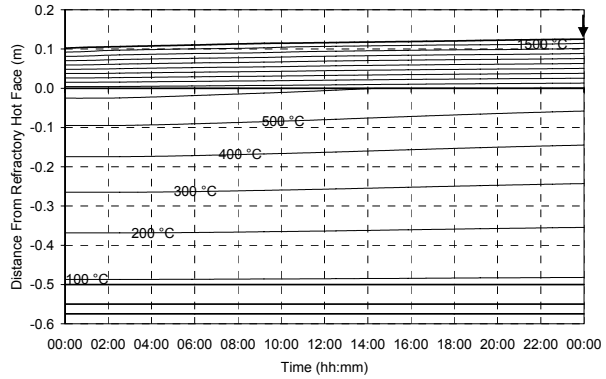

(a)

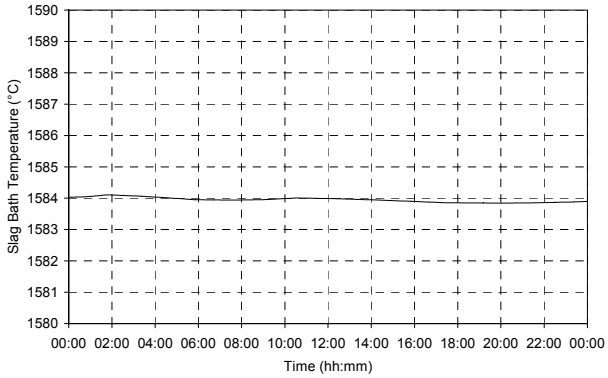

(b)

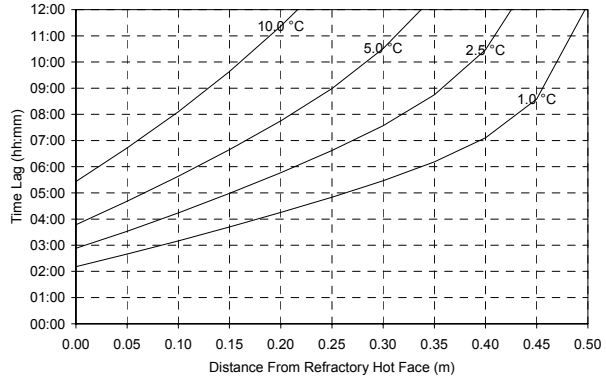

(c)

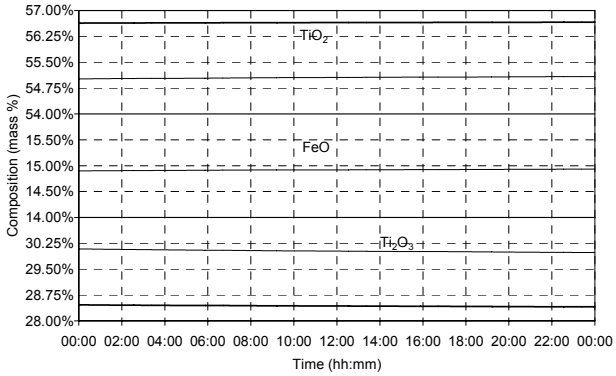

(d)

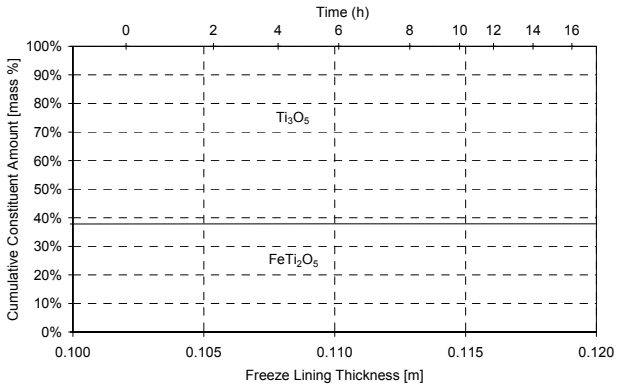

(e)

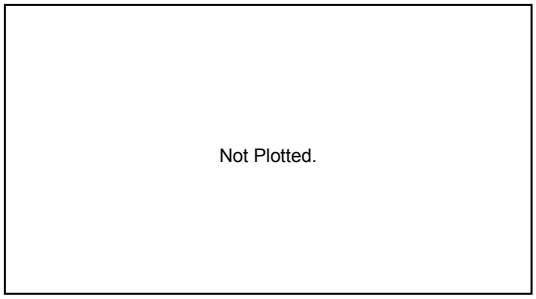

(f)

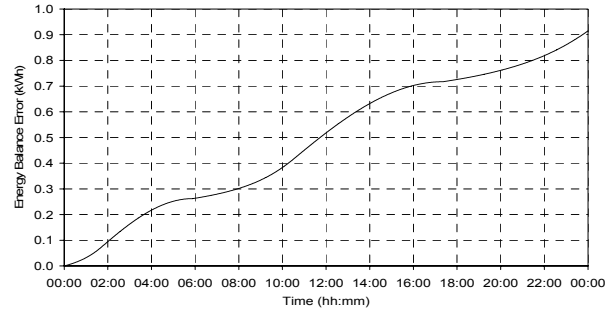

(g)

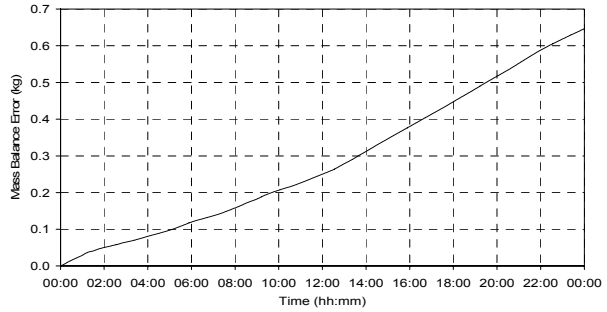

(h)

Figure 66 – Experiment 6.7 results.

6.3.8 Experiment 6.8

INITIAL STEADY STATE HEAT FLOW	INITIAL FREEZE LINING THICKNESS	INITIAL FREEZE LINING COMPOSITION	ELECTRICAL POWER HEAT FLOW	HEAT LOSSES HEAT FLOW	NET INPUT HEAT FLOW
250 kW	0.102 m	Pseudobrookite	300 kW	0 kW	300 kW

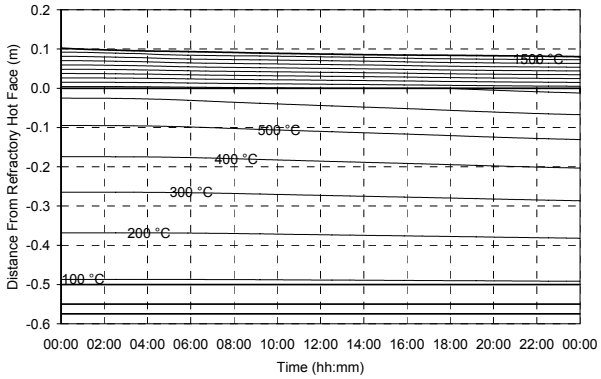

(a)

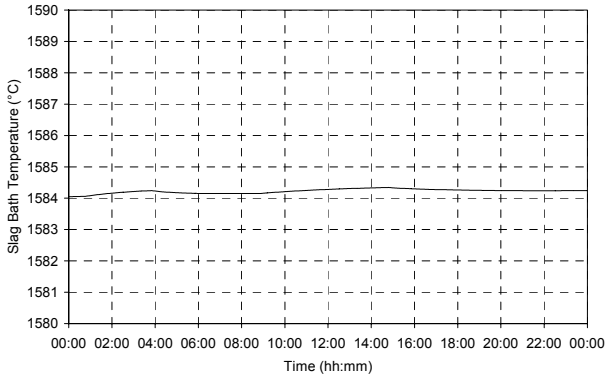

(b)

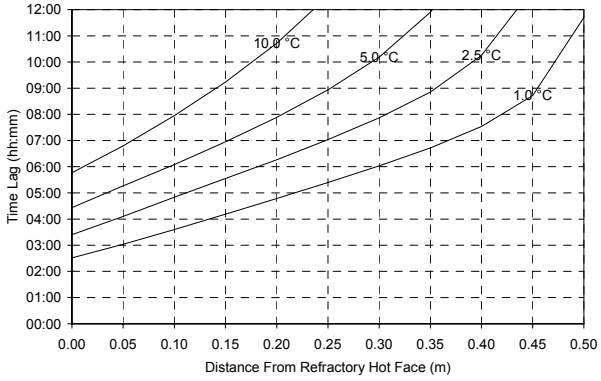

(c)

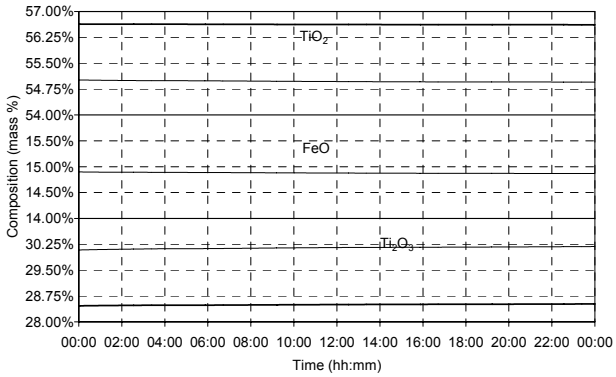

(d)

Not Plotted.

(e)

Not Plotted.

(f)

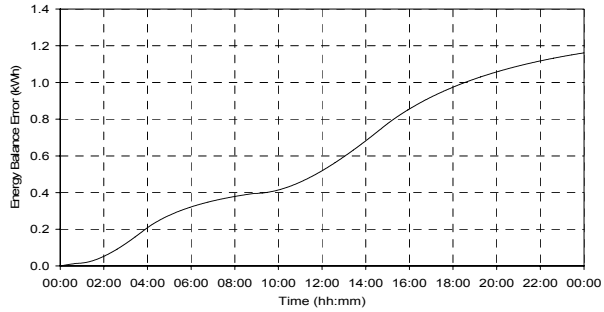

(g)

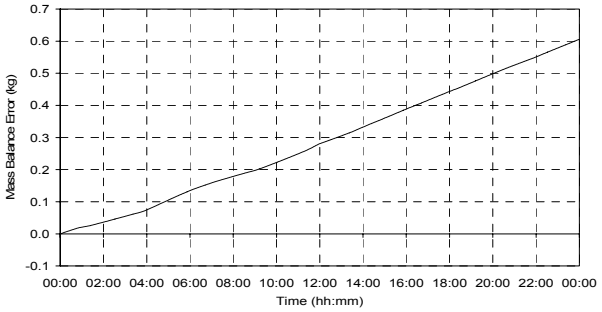

(h)

Figure 67 – Experiment 6.8 results.

6.3.9 Experiment 6.9

INITIAL STEADY STATE HEAT FLOW	INITIAL FREEZE LINING THICKNESS	INITIAL FREEZE LINING COMPOSITION	ELECTRICAL POWER HEAT FLOW	HEAT LOSSES HEAT FLOW	NET INPUT HEAT FLOW
250 kW	0.102 m	Pseudobrookite	400 kW	0 kW	400 kW

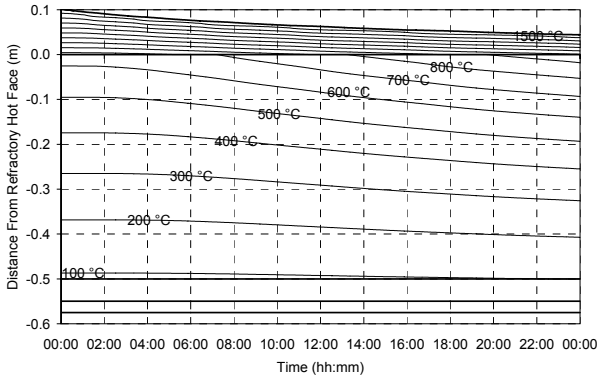

(a)

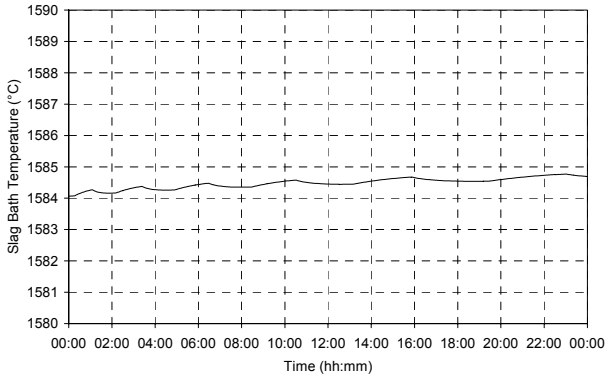

(b)

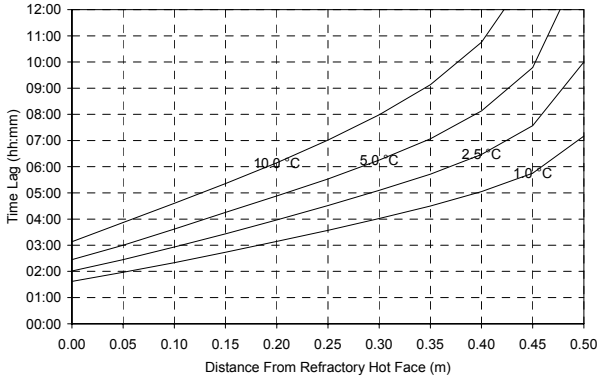

(c)

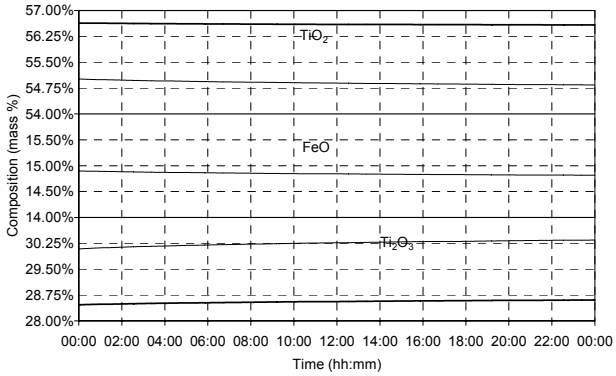

(d)

Not Plotted.

(e)

Not Plotted.

(f)

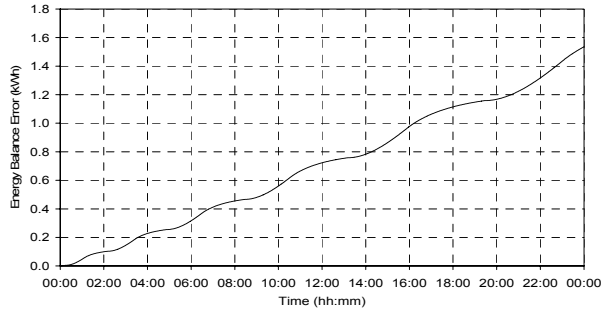

(g)

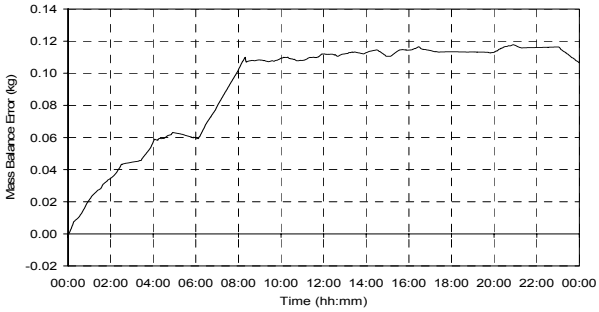

(h)

Figure 68 – Experiment 6.9 results.

6.3.10 Experiment 6.10

INITIAL STEADY STATE HEAT FLOW	INITIAL FREEZE LINING THICKNESS	INITIAL FREEZE LINING COMPOSITION	ELECTRICAL POWER HEAT FLOW	HEAT LOSSES HEAT FLOW	NET INPUT HEAT FLOW
250 kW	0.102 m	Pseudobrookite	500 kW	0 kW	500 kW

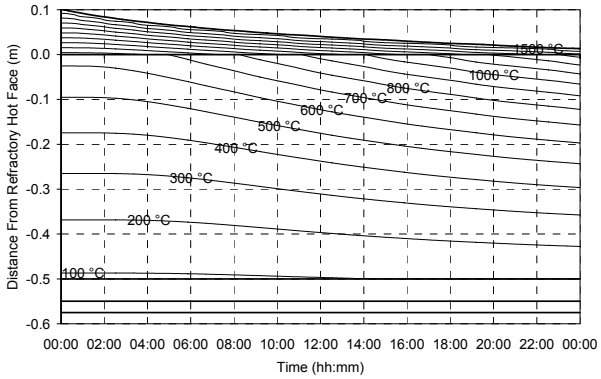

(a)

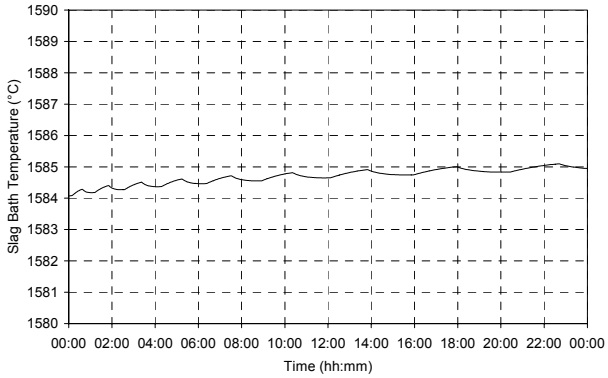

(b)

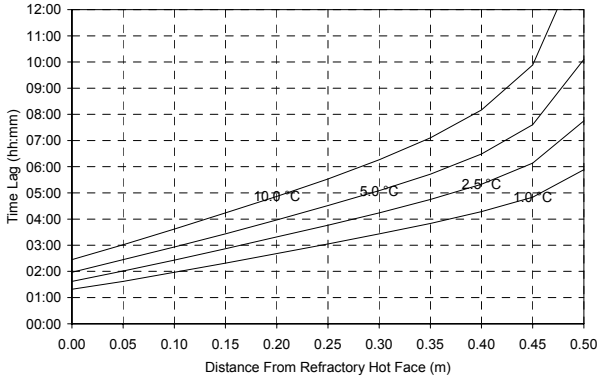

(c)

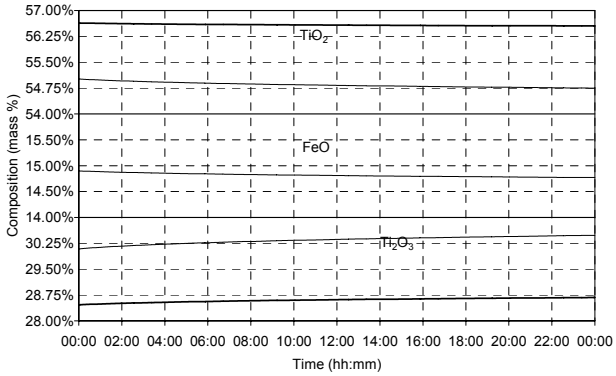

(d)

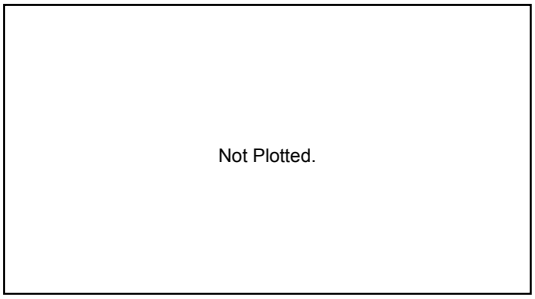

(e)

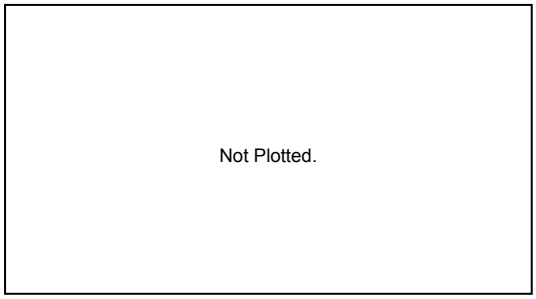

(f)

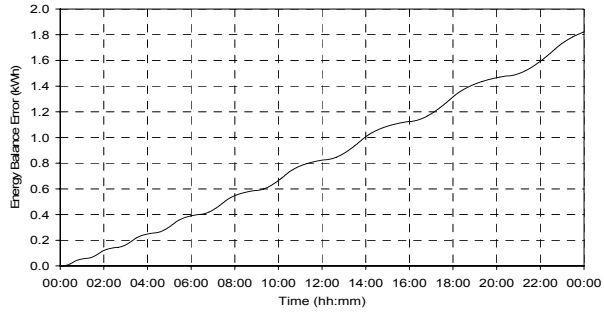

(g)

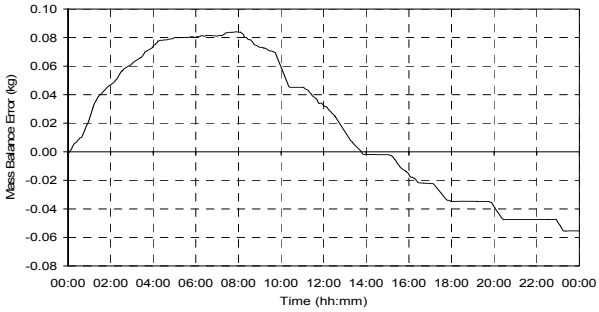

(h)

Figure 69 – Experiment 6.10 results.

6.3.11 Experiment 6.11

INITIAL STEADY STATE HEAT FLOW	INITIAL FREEZE LINING THICKNESS	INITIAL FREEZE LINING COMPOSITION	ELECTRICAL POWER HEAT FLOW	HEAT LOSSES HEAT FLOW	NET INPUT HEAT FLOW
250 kW	0.102 m	Pseudobrookite	1000 kW	0 kW	1000 kW

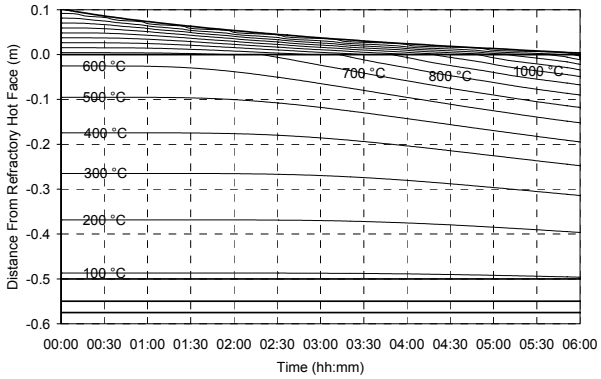

(a)

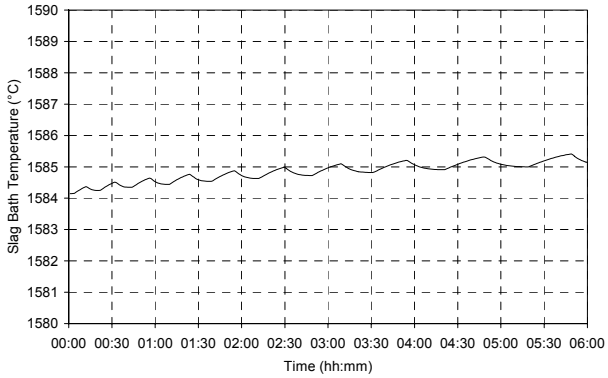

(b)

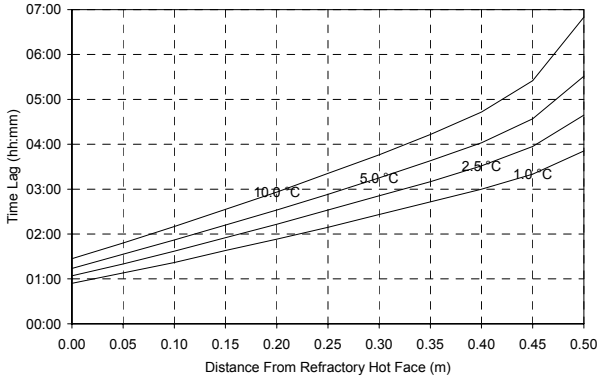

(c)

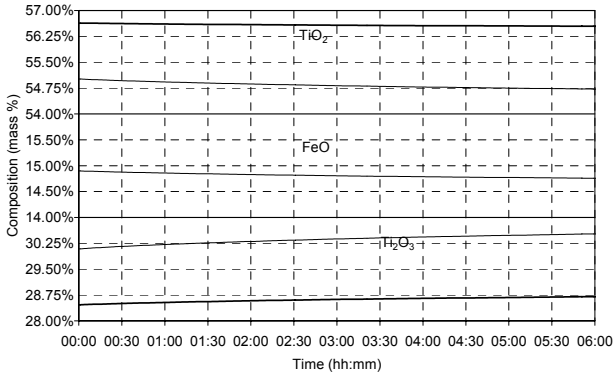

(d)

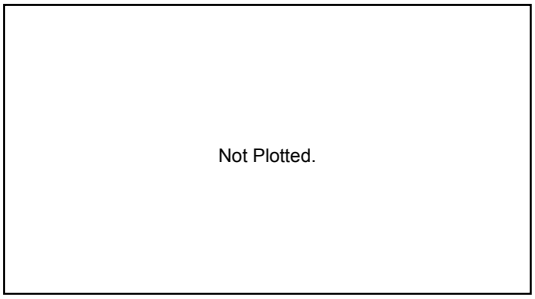

(e)

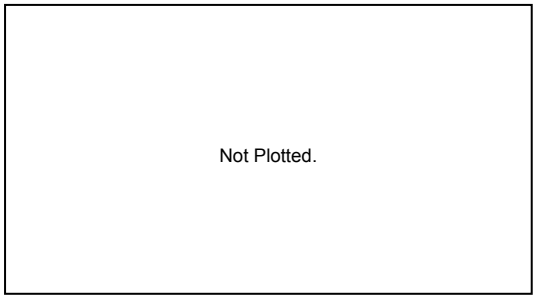

(f)

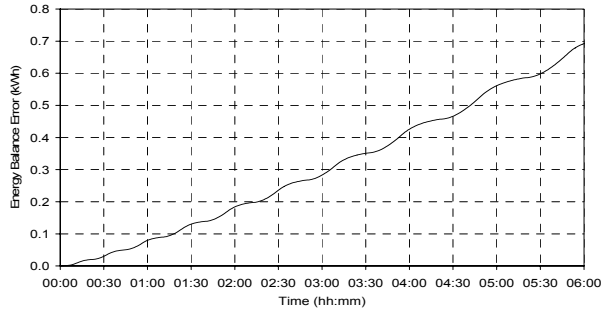

(g)

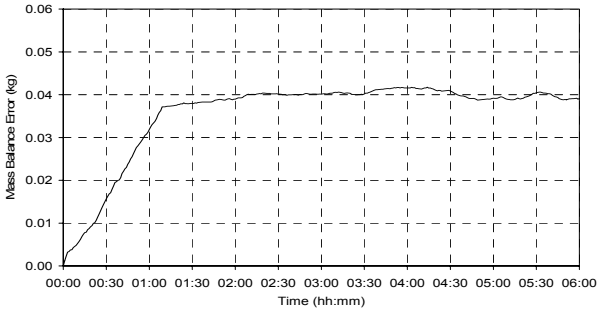

(h)

Figure 70 – Experiment 6.11 results.

6.3.12 Experiment 6.12

INITIAL STEADY STATE HEAT FLOW	INITIAL FREEZE LINING THICKNESS	INITIAL FREEZE LINING COMPOSITION	ELECTRICAL POWER HEAT FLOW	HEAT LOSSES HEAT FLOW	NET INPUT HEAT FLOW
250 kW	0.102 m	Pseudobrookite	2000 kW	0 kW	2000 kW

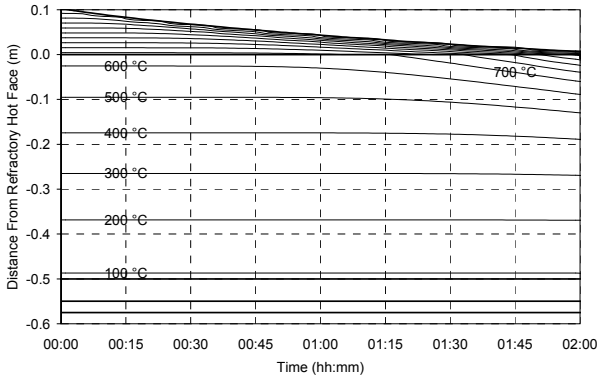

(a)

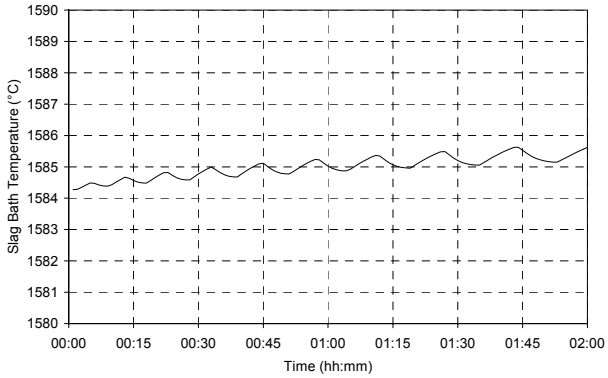

(b)

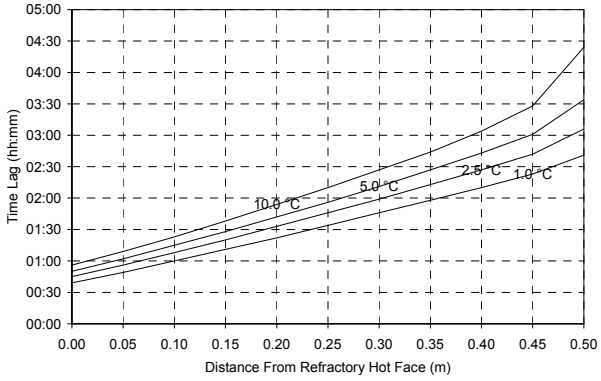

(c)

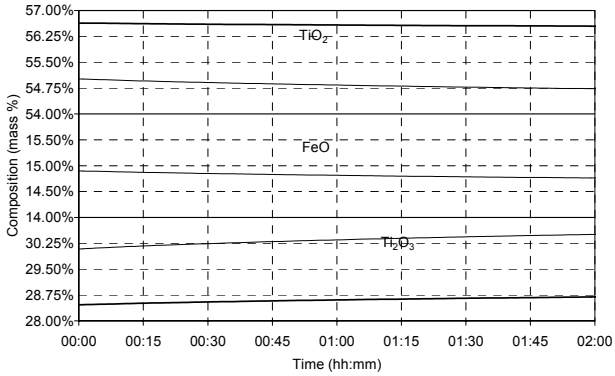

(d)

Not Plotted.

(e)

Not Plotted.

(f)

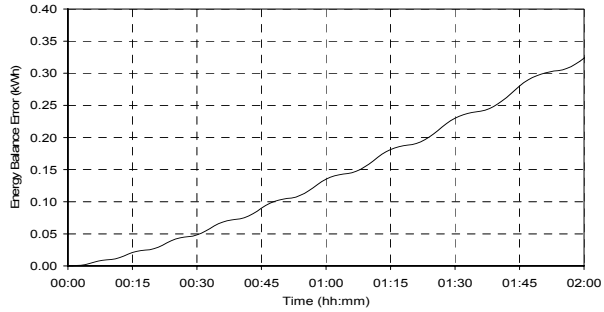

(g)

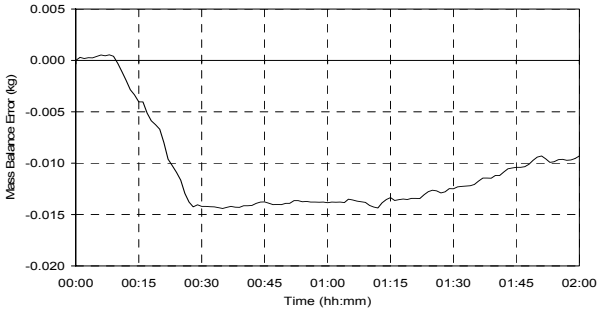

(h)

Figure 71 – Experiment 6.12 results.

6.3.13 Experiment 6.13

INITIAL STEADY STATE HEAT FLOW	INITIAL FREEZE LINING THICKNESS	INITIAL FREEZE LINING COMPOSITION	ELECTRICAL POWER HEAT FLOW	HEAT LOSSES HEAT FLOW	NET INPUT HEAT FLOW
250 kW	0.102 m	Pseudobrookite	5000 kW	0 kW	5000 kW

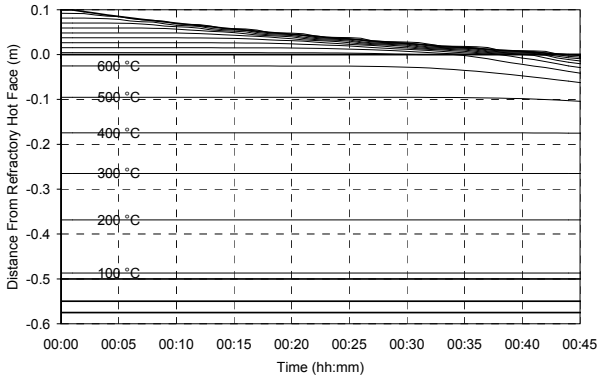

(a)

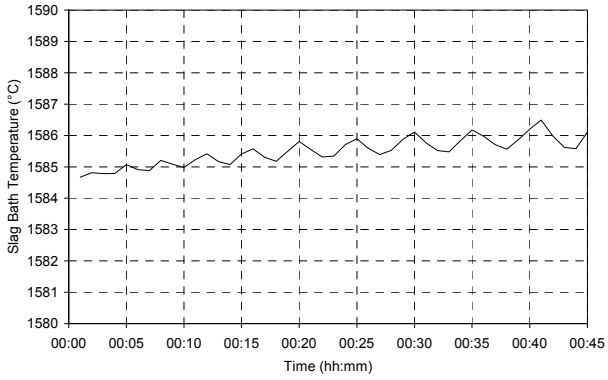

(b)

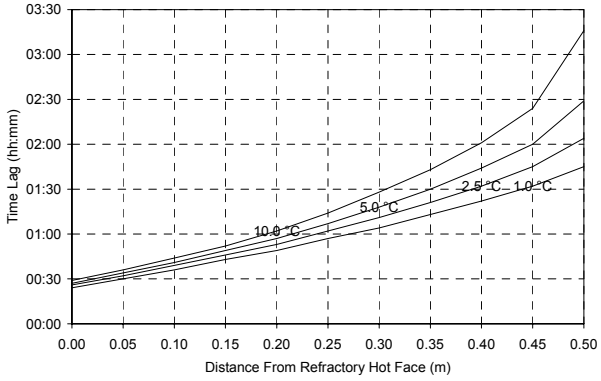

(c)

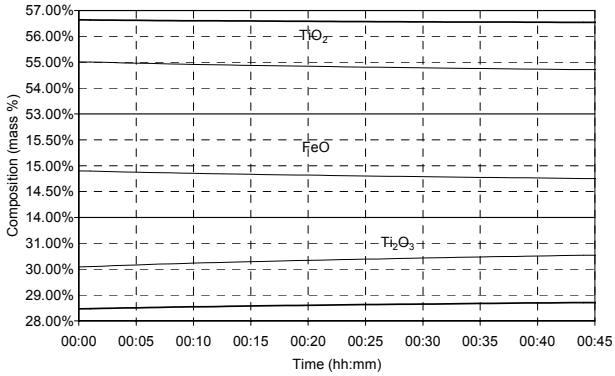

(d)

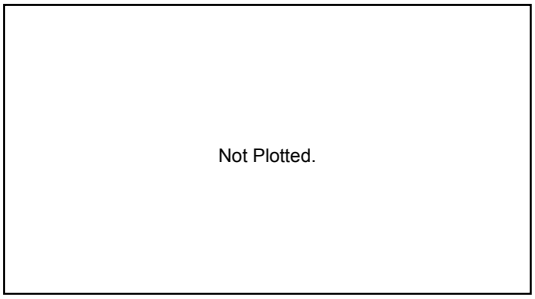

(e)

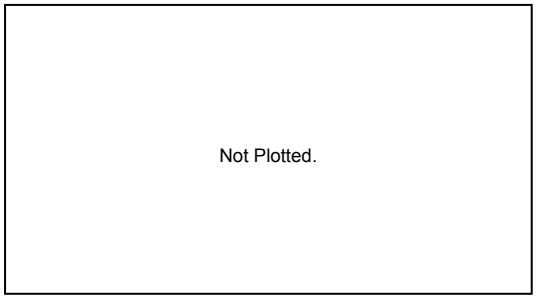

(f)

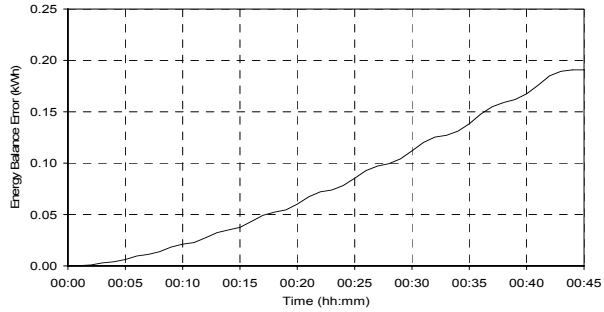

(g)

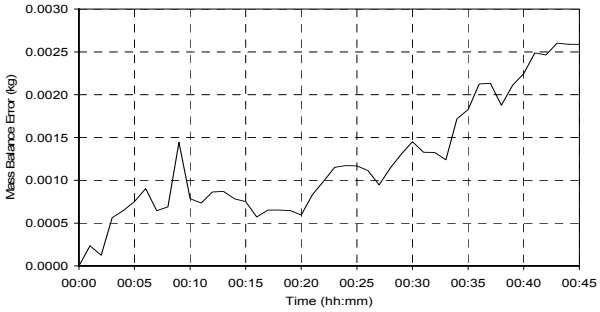

(h)

Figure 72 – Experiment 6.13 results.

6.3.14 Experiment 6.14

INITIAL STEADY STATE HEAT FLOW	INITIAL FREEZE LINING THICKNESS	INITIAL FREEZE LINING COMPOSITION	ELECTRICAL POWER HEAT FLOW	HEAT LOSSES HEAT FLOW	NET INPUT HEAT FLOW
250 kW	0.102 m	Pseudobrookite	10000 kW	0 kW	10000 kW

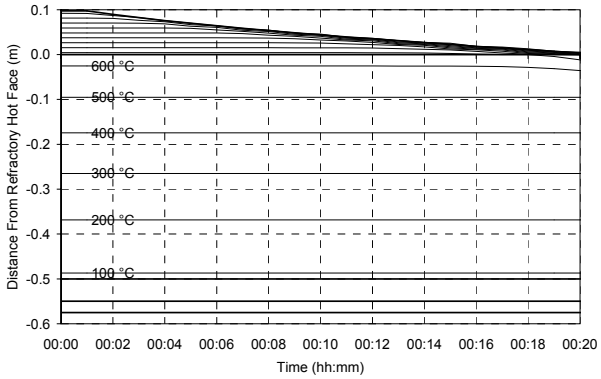

(a)

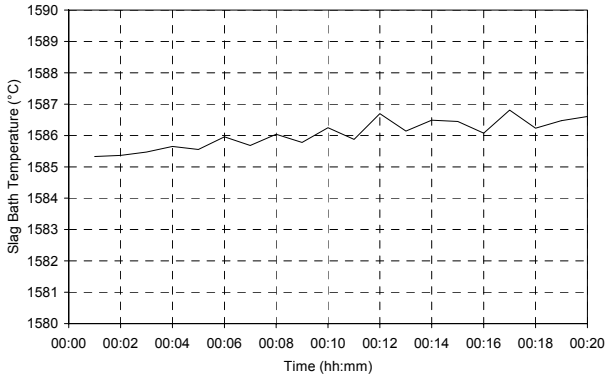

(b)

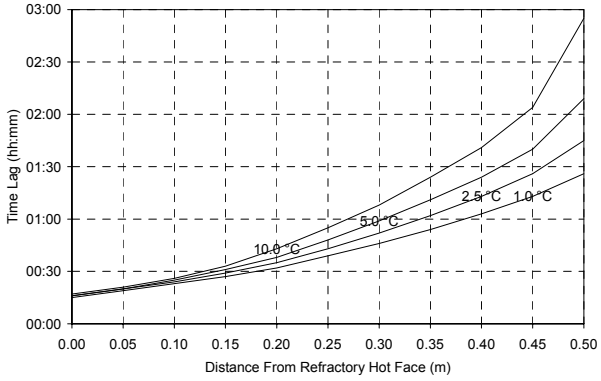

(c)

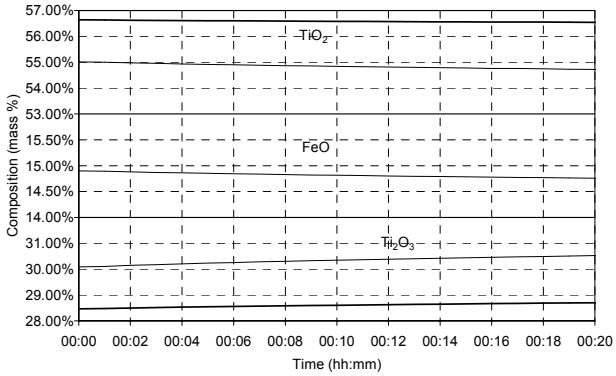

(d)

Not Plotted.

(e)

Not Plotted.

(f)

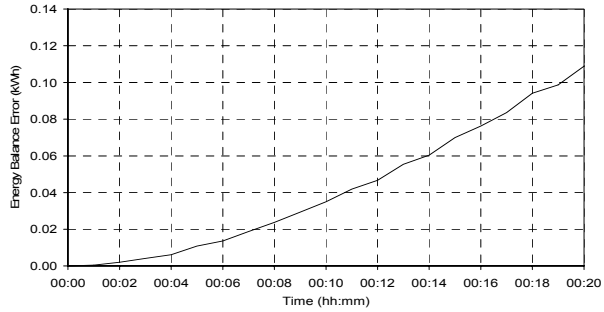

(g)

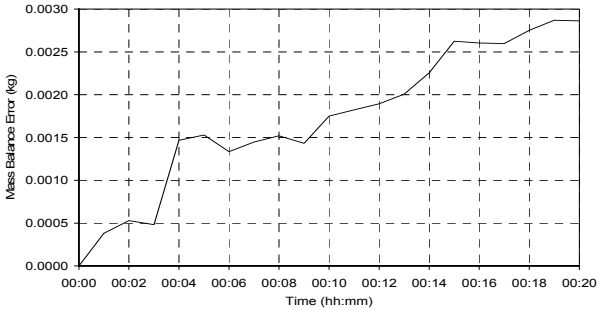

(h)

Figure 73 – Experiment 6.14 results.

6.3.15 Experiment 6.15

INITIAL STEADY STATE HEAT FLOW	INITIAL FREEZE LINING THICKNESS	INITIAL FREEZE LINING COMPOSITION	ELECTRICAL POWER HEAT FLOW	HEAT LOSSES HEAT FLOW	NET INPUT HEAT FLOW
300 kW	0.066 m	Pseudobrookite	0 kW	1000 kW	-1000 kW

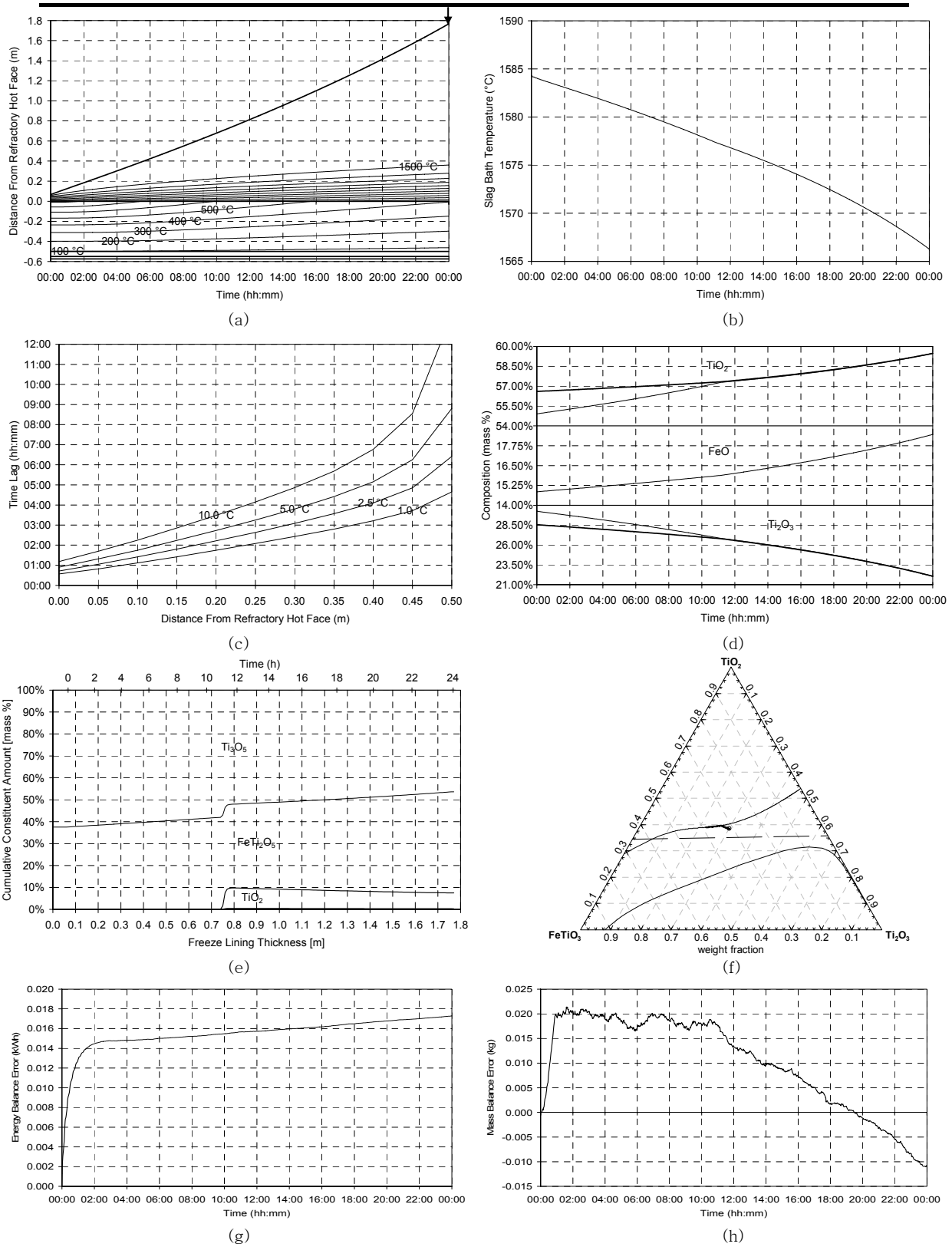

Figure 74 – Experiment 6.15 results.

6.3.16 Experiment 6.16

INITIAL STEADY STATE HEAT FLOW	INITIAL FREEZE LINING THICKNESS	INITIAL FREEZE LINING COMPOSITION	ELECTRICAL POWER HEAT FLOW	HEAT LOSSES HEAT FLOW	NET INPUT HEAT FLOW
300 kW	0.066 m	Pseudobrookite	0 kW	0 kW	0 kW

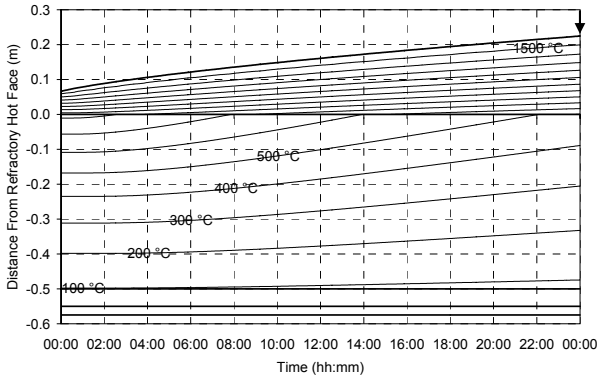

(a)

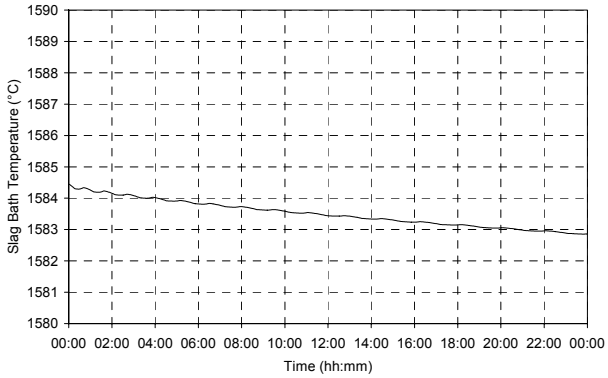

(b)

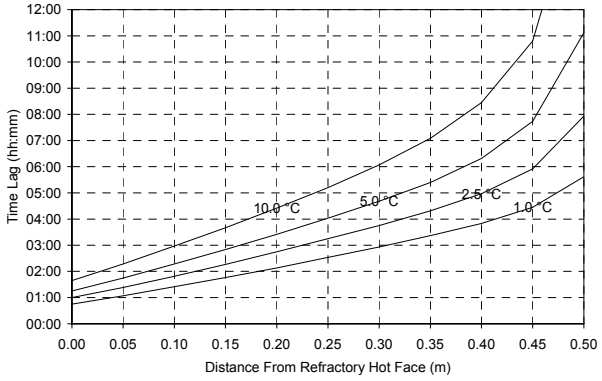

(c)

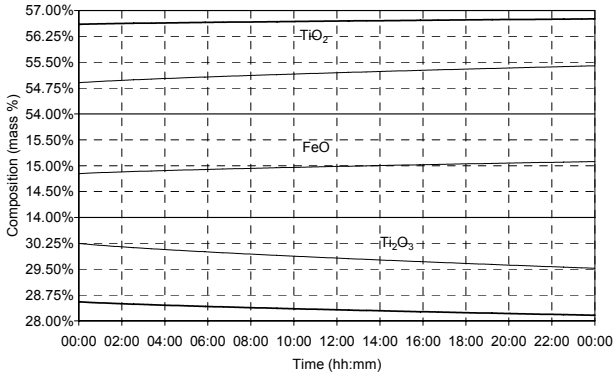

(d)

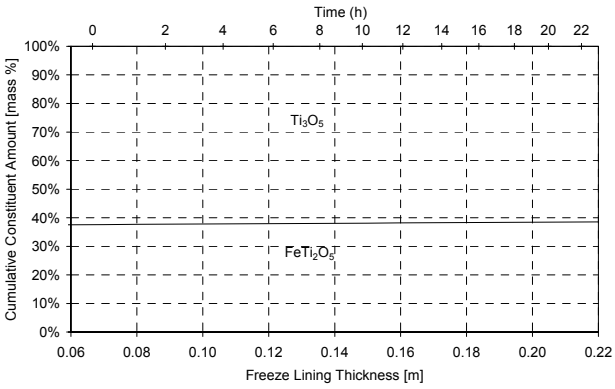

(e)

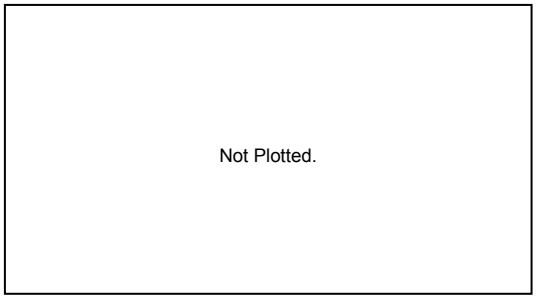

(f)

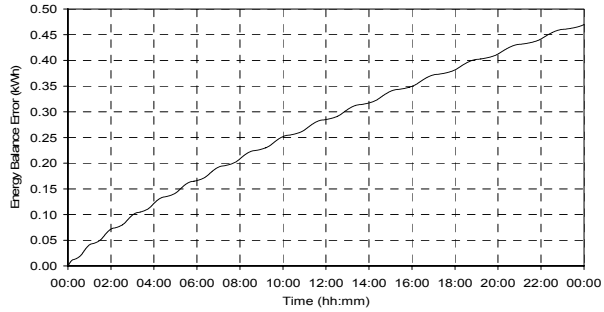

(g)

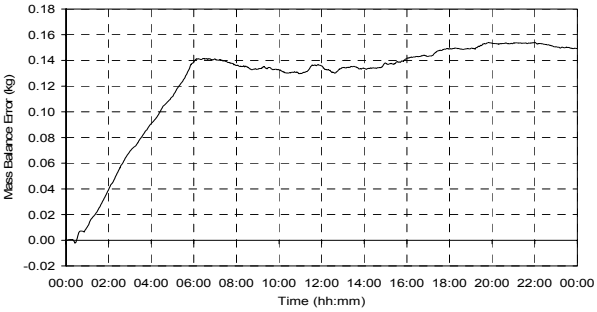

(h)

Figure 75 – Experiment 6.16 results.

6.3.17 Experiment 6.17

INITIAL STEADY STATE HEAT FLOW	INITIAL FREEZE LINING THICKNESS	INITIAL FREEZE LINING COMPOSITION	ELECTRICAL POWER HEAT FLOW	HEAT LOSSES HEAT FLOW	NET INPUT HEAT FLOW
300 kW	0.066 m	Pseudobrookite	200 kW	0 kW	200 kW

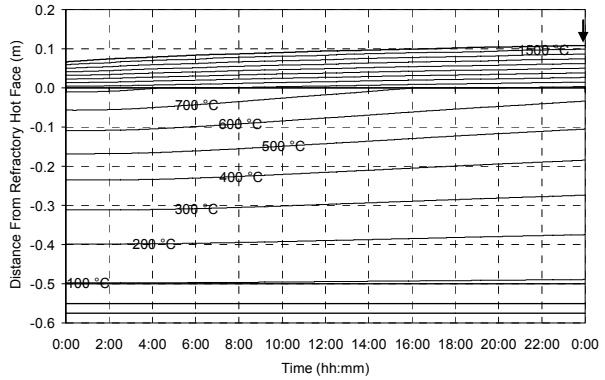

(a)

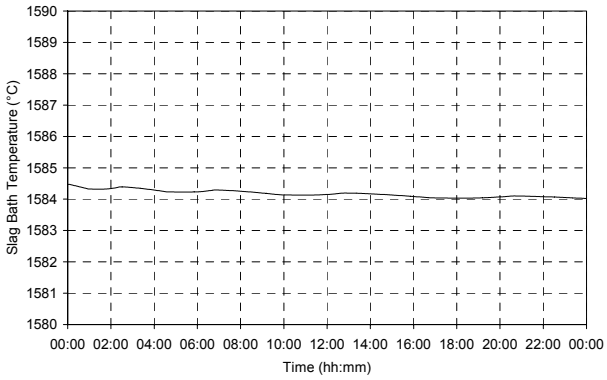

(b)

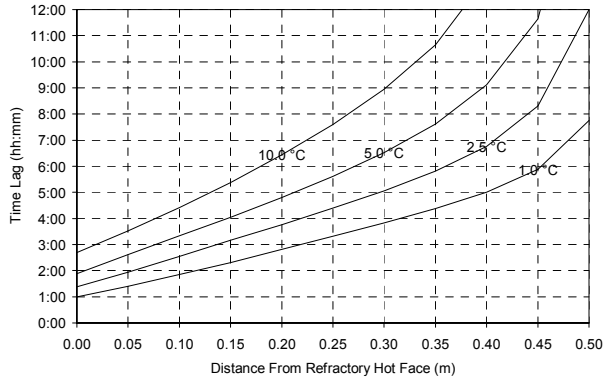

(c)

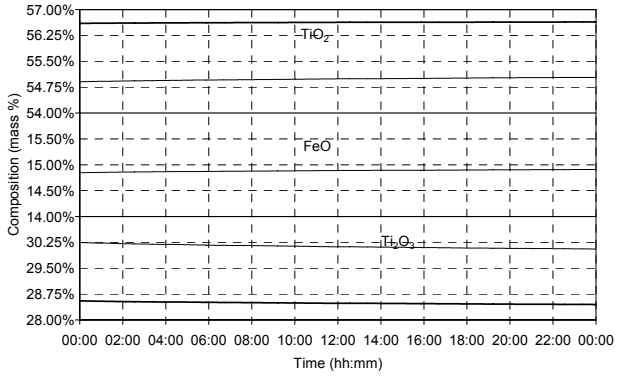

(d)

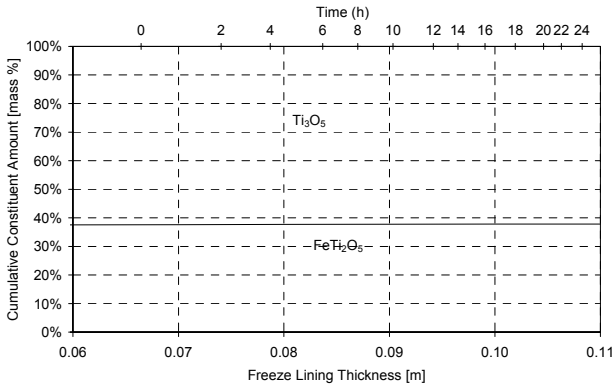

(e)

Not Plotted.

(f)

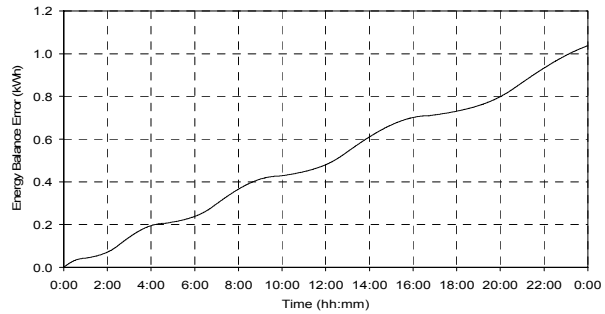

(g)

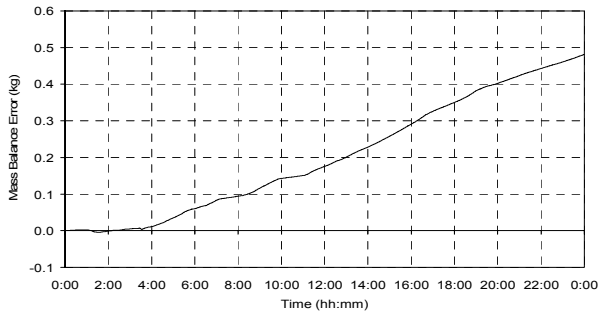

(h)

Figure 76 – Experiment 6.17 results.

6.3.18 Experiment 6.18

INITIAL STEADY STATE HEAT FLOW	INITIAL FREEZE LINING THICKNESS	INITIAL FREEZE LINING COMPOSITION	ELECTRICAL POWER HEAT FLOW	HEAT LOSSES HEAT FLOW	NET INPUT HEAT FLOW
300 kW	0.066 m	Pseudobrookite	400 kW	0 kW	400 kW

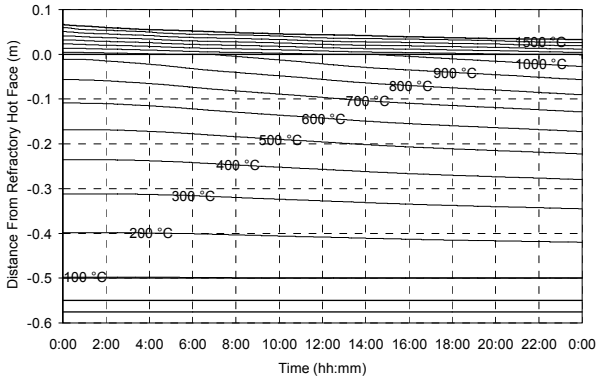

(a)

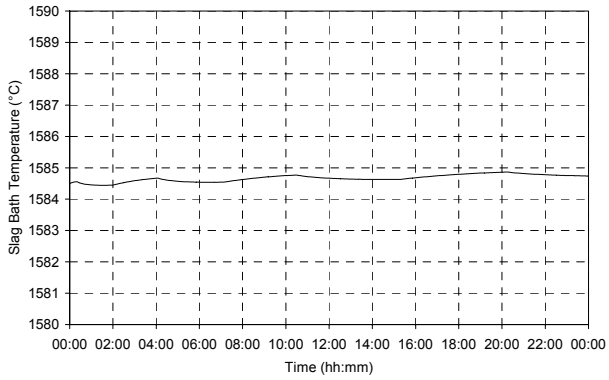

(b)

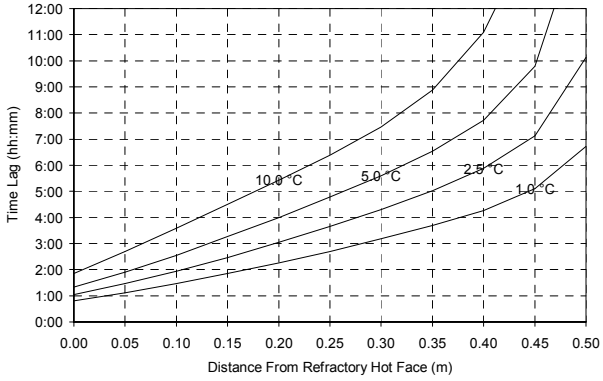

(c)

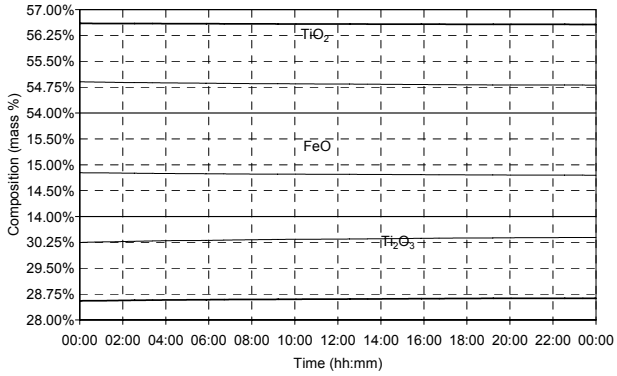

(d)

Not Plotted.

(e)

Not Plotted.

(f)

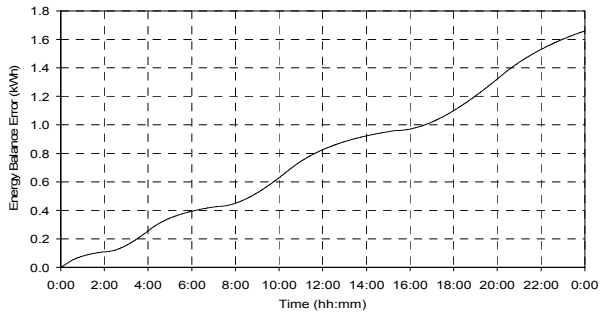

(g)

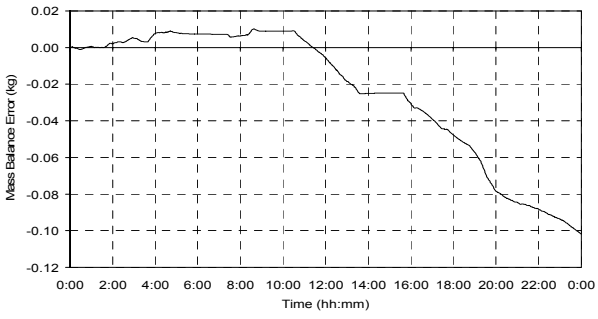

(h)

Figure 77 – Experiment 6.18 results.

6.3.19 Experiment 6.19

INITIAL STEADY STATE HEAT FLOW	INITIAL FREEZE LINING THICKNESS	INITIAL FREEZE LINING COMPOSITION	ELECTRICAL POWER HEAT FLOW	HEAT LOSSES HEAT FLOW	NET INPUT HEAT FLOW
300 kW	0.066 m	Pseudobrookite	1000 kW	0 kW	1000 kW

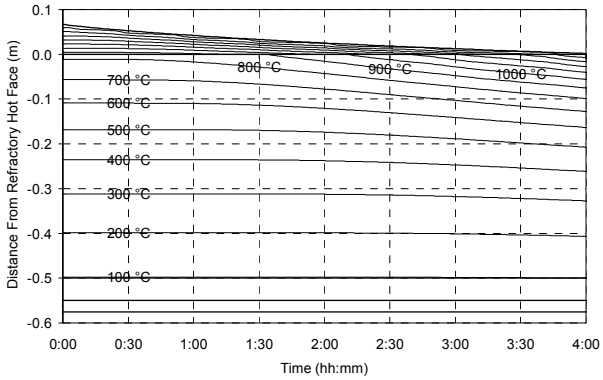

(a)

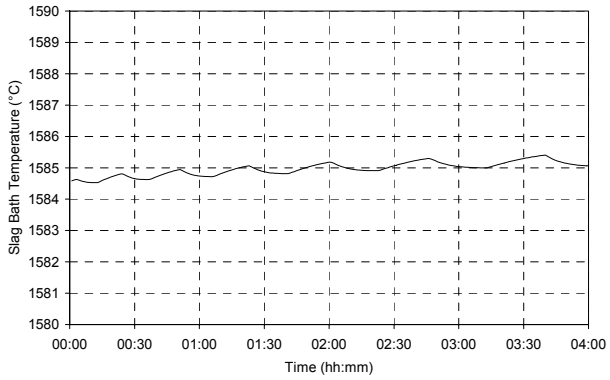

(b)

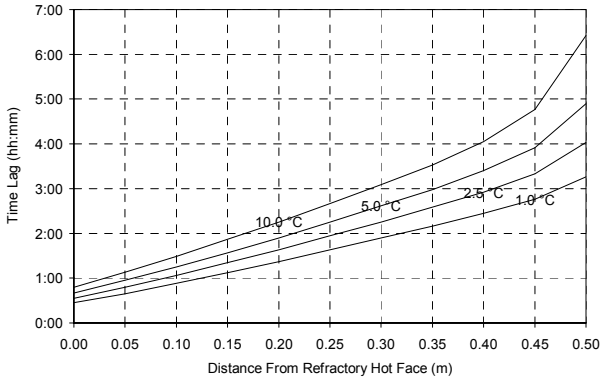

(c)

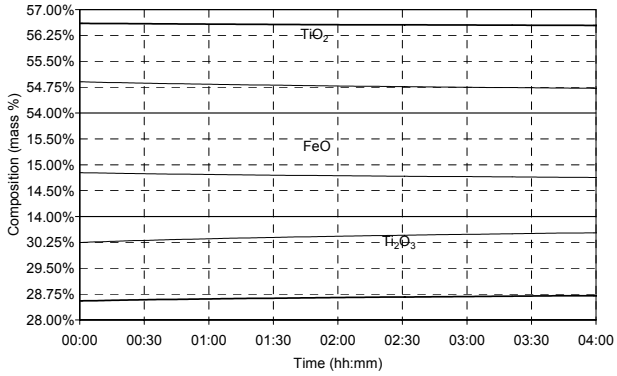

(d)

Not Plotted.

(e)

Not Plotted.

(f)

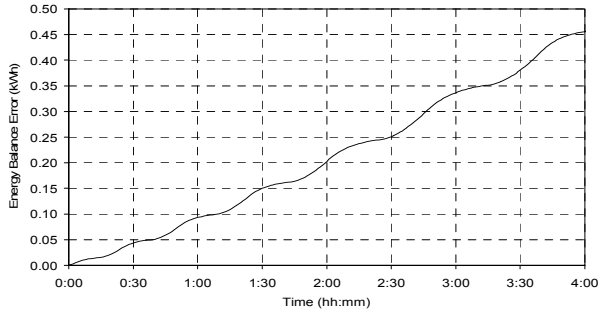

(g)

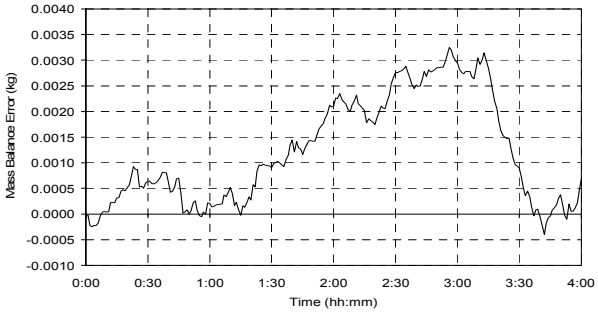

(h)

Figure 78 – Experiment 6.19 results.

6.3.20 Experiment 6.20

INITIAL STEADY STATE HEAT FLOW	INITIAL FREEZE LINING THICKNESS	INITIAL FREEZE LINING COMPOSITION	ELECTRICAL POWER HEAT FLOW	HEAT LOSSES HEAT FLOW	NET INPUT HEAT FLOW
300 kW	0.066 m	Pseudobrookite	10000 kW	0 kW	10000 kW

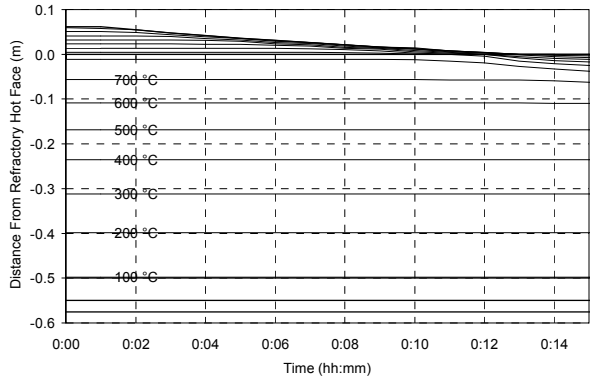

(a)

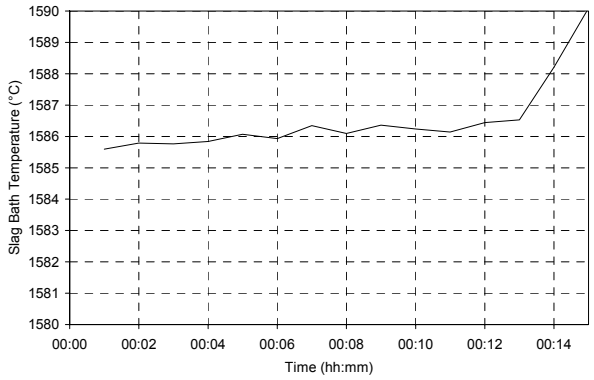

(b)

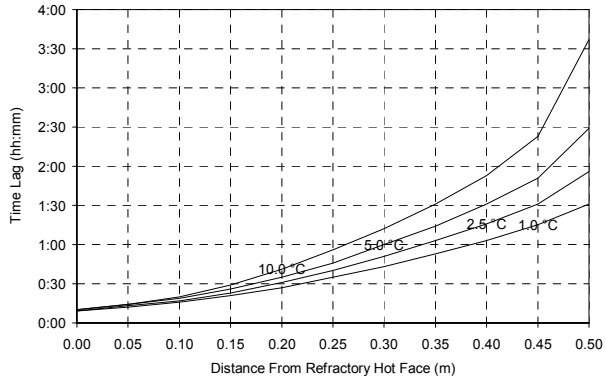

(c)

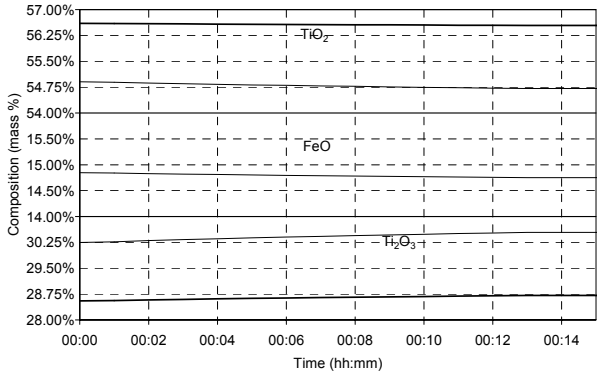

(d)

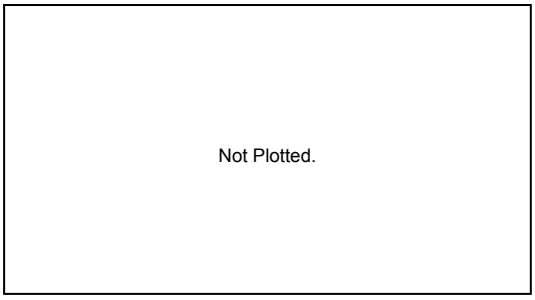

(e)

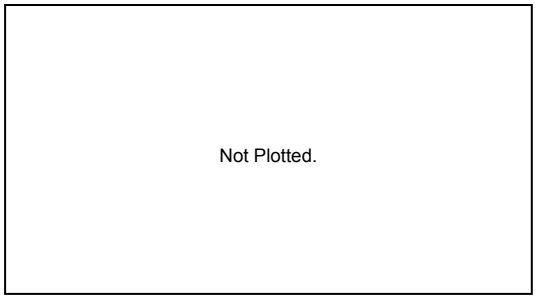

(f)

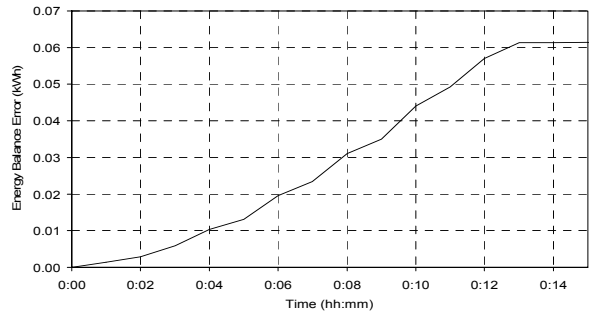

(g)

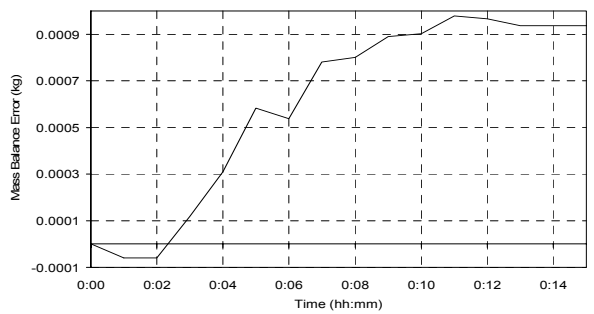

(h)

Figure 79 – Experiment 6.20 results.

6.3.21 Experiment 6.21

INITIAL STEADY STATE HEAT FLOW	INITIAL FREEZE LINING THICKNESS	INITIAL FREEZE LINING COMPOSITION	ELECTRICAL POWER HEAT FLOW	HEAT LOSSES HEAT FLOW	NET INPUT HEAT FLOW
250 kW	0.102 m	Rutile	0 kW	1000 kW	-1000 kW

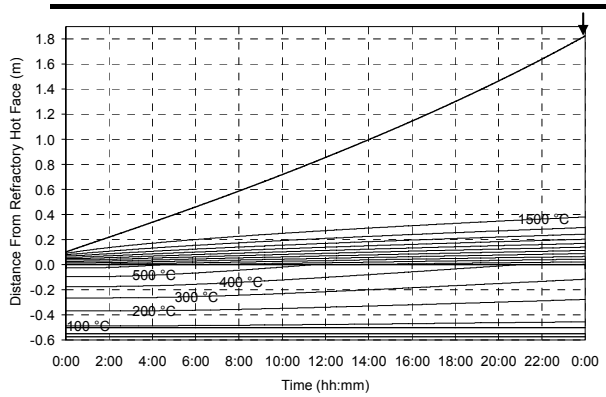

(a)

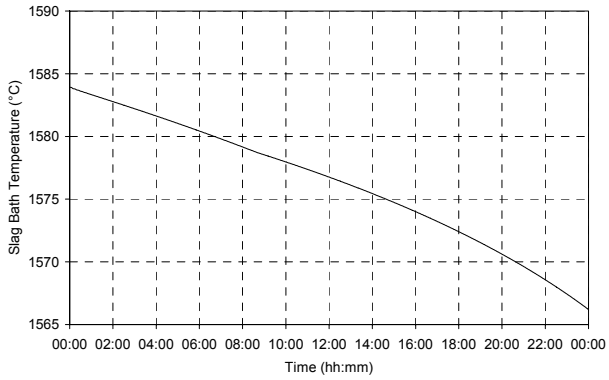

(b)

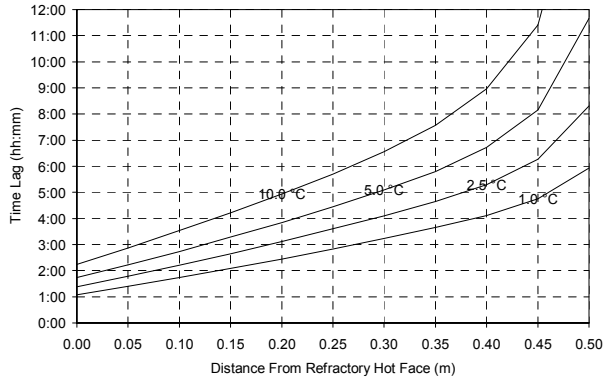

(c)

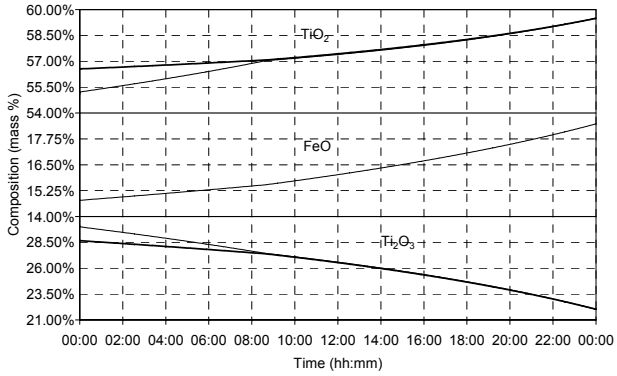

(d)

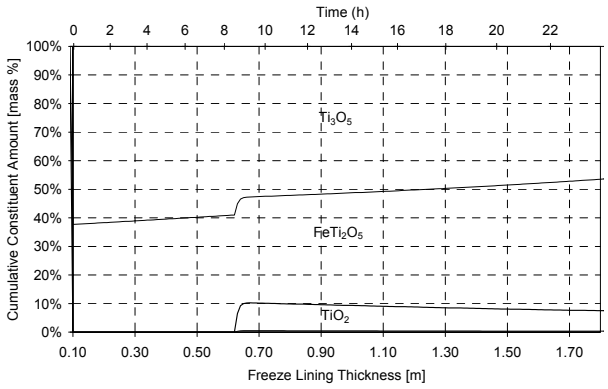

(e)

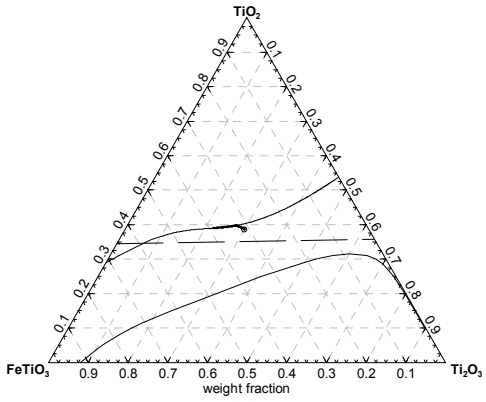

(f)

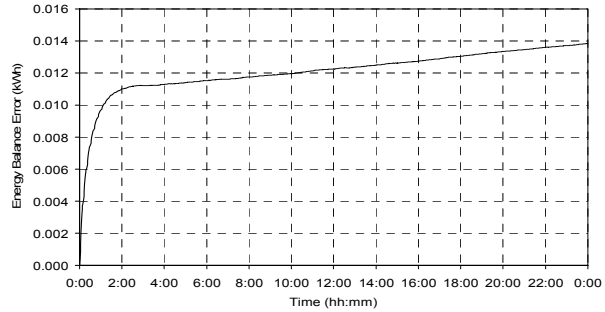

(g)

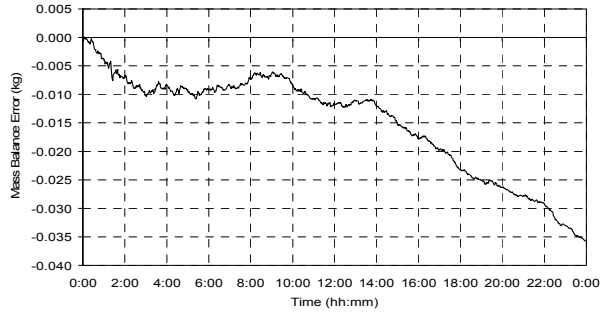

(h)

Figure 80 – Experiment 6.21 results.

6.3.22 Experiment 6.22

INITIAL STEADY STATE HEAT FLOW	INITIAL FREEZE LINING THICKNESS	INITIAL FREEZE LINING COMPOSITION	ELECTRICAL POWER HEAT FLOW	HEAT LOSSES HEAT FLOW	NET INPUT HEAT FLOW
250 kW	0.102 m	Rutile	0 kW	0 kW	0 kW

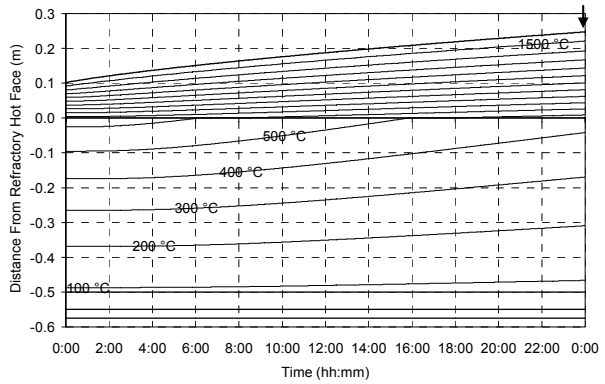

(a)

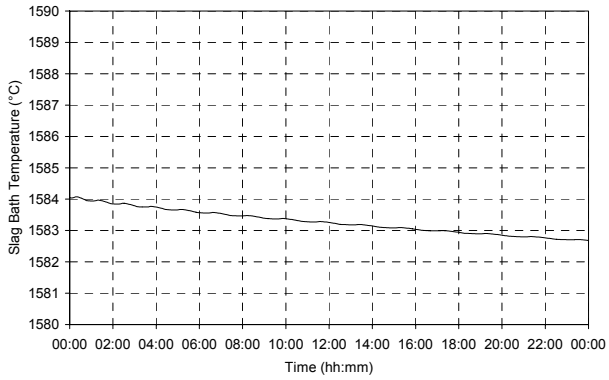

(b)

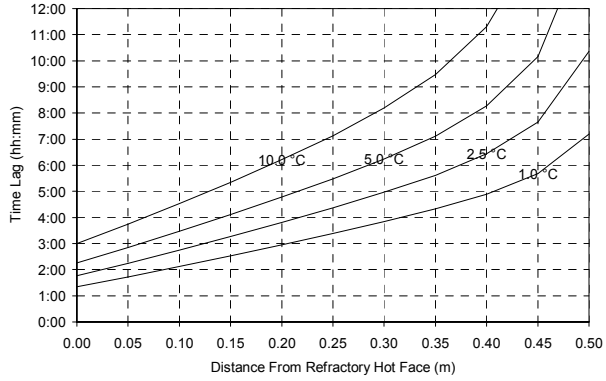

(c)

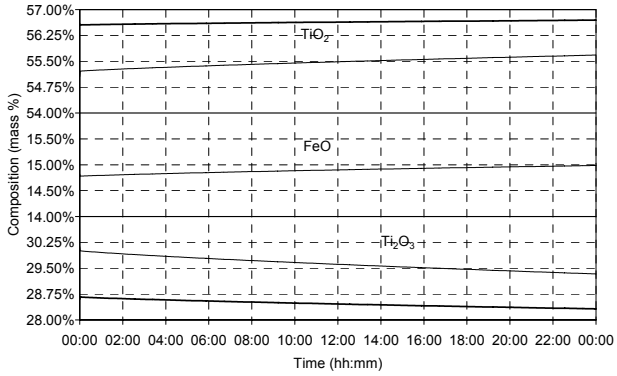

(d)

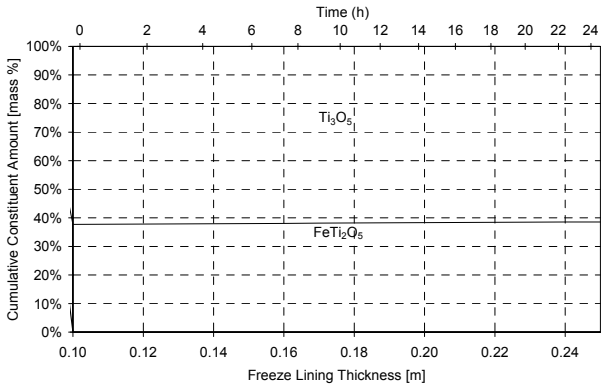

(e)

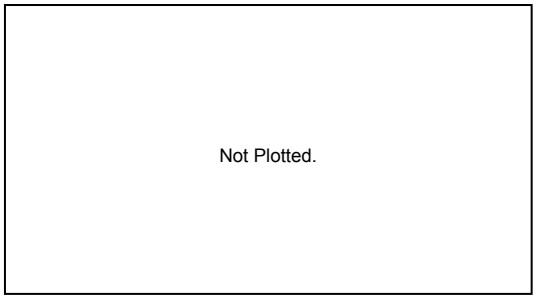

(f)

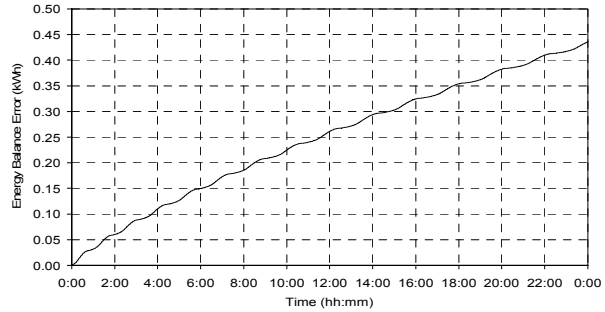

(g)

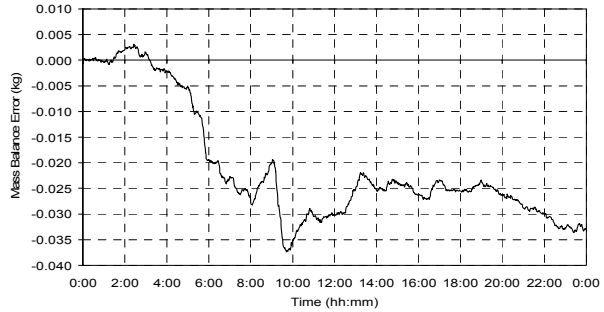

(h)

Figure 81 – Experiment 6.22 results.

6.3.23 Experiment 6.23

INITIAL STEADY STATE HEAT FLOW	INITIAL FREEZE LINING THICKNESS	INITIAL FREEZE LINING COMPOSITION	ELECTRICAL POWER HEAT FLOW	HEAT LOSSES HEAT FLOW	NET INPUT HEAT FLOW
250 kW	0.102 m	Rutile	200 kW	0 kW	200 kW

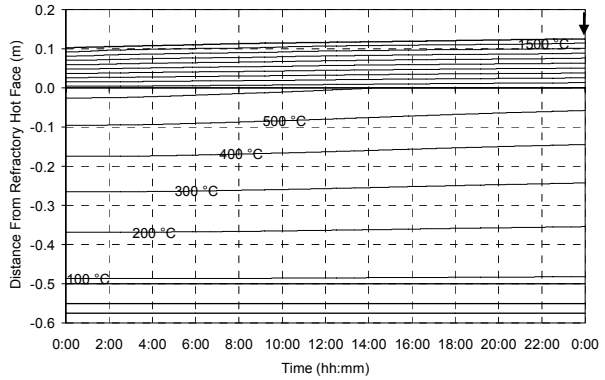

(a)

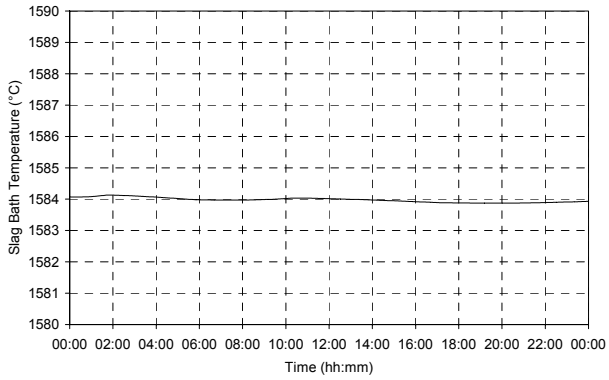

(b)

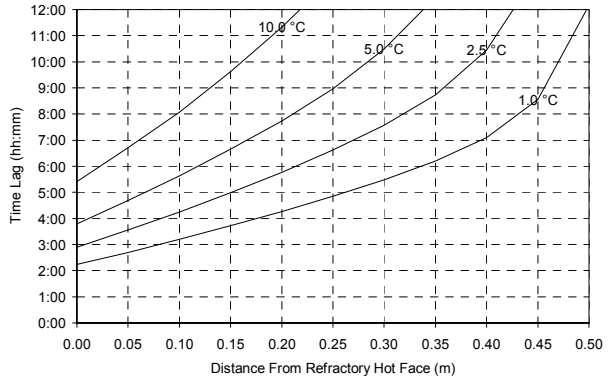

(c)

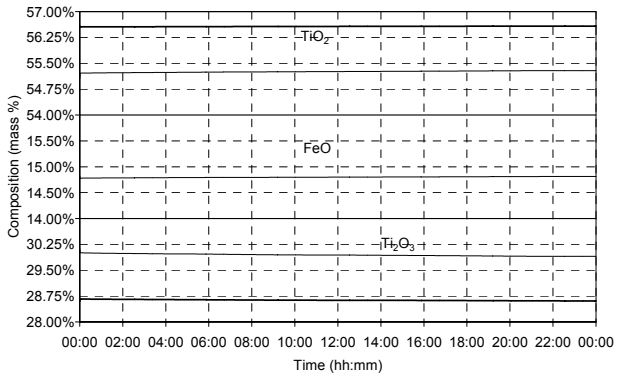

(d)

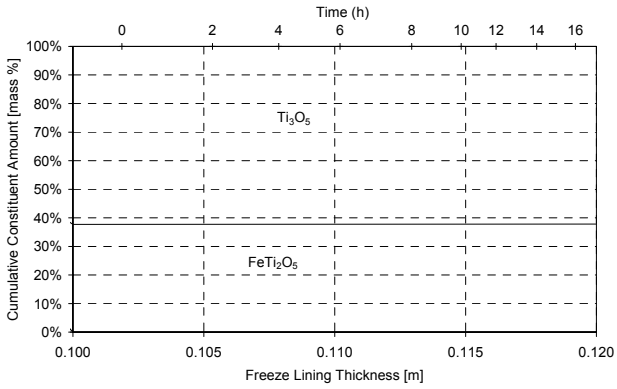

(e)

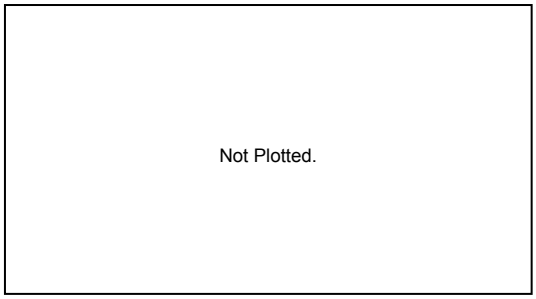

(f)

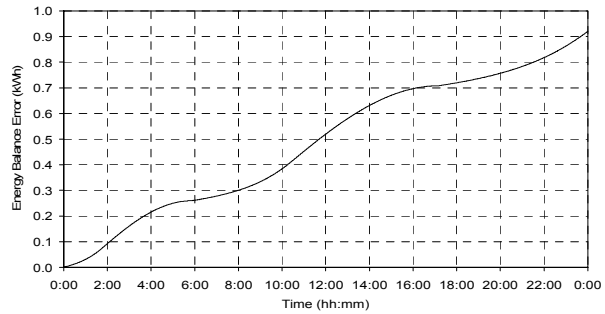

(g)

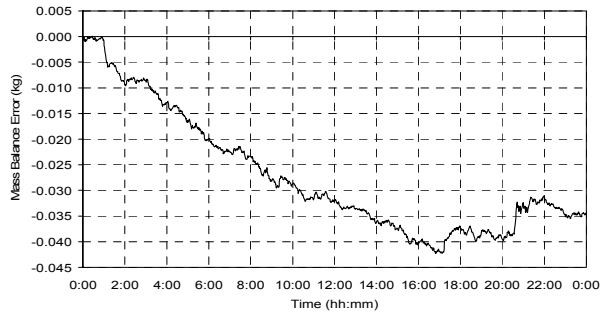

(h)

Figure 82 – Experiment 6.23 results.

6.3.24 Experiment 6.24

INITIAL STEADY STATE HEAT FLOW	INITIAL FREEZE LINING THICKNESS	INITIAL FREEZE LINING COMPOSITION	ELECTRICAL POWER HEAT FLOW	HEAT LOSSES HEAT FLOW	NET INPUT HEAT FLOW
250 kW	0.102 m	Rutile	400 kW	0 kW	400 kW

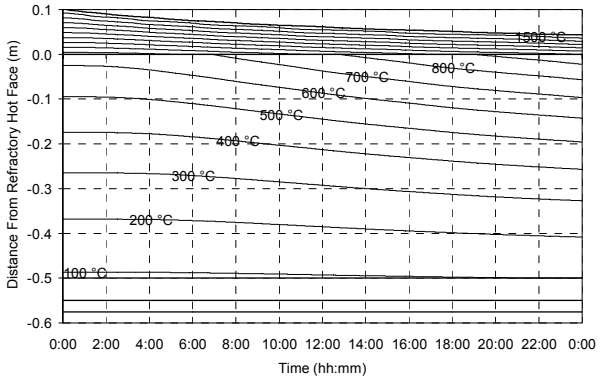

(a)

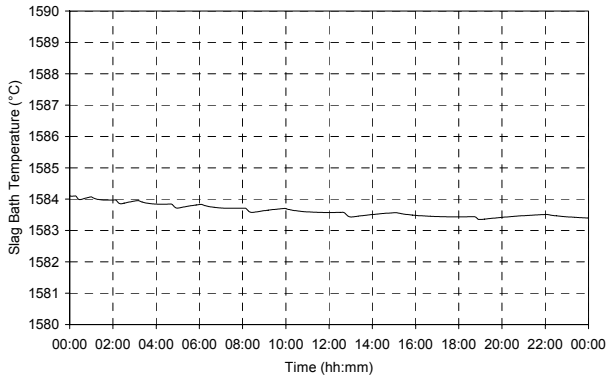

(b)

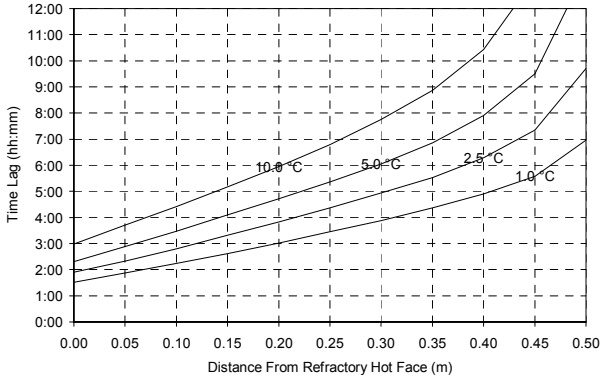

(c)

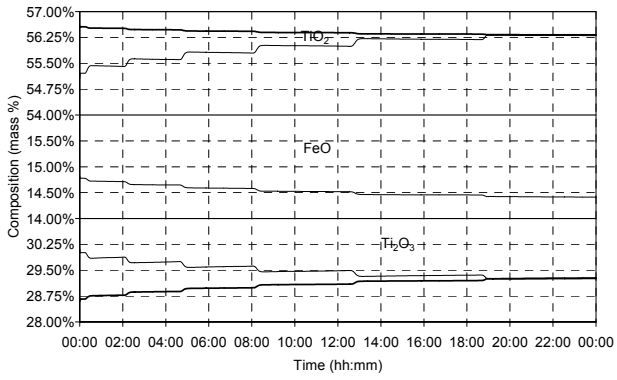

(d)

Not Plotted.

(e)

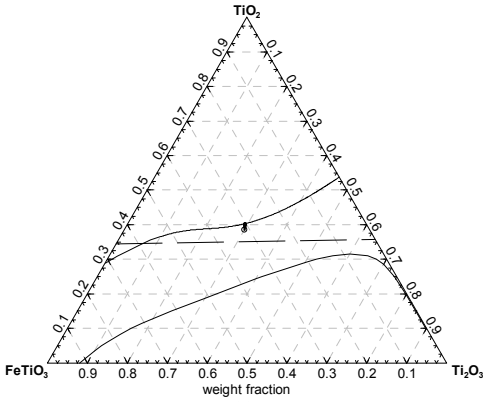

(f)

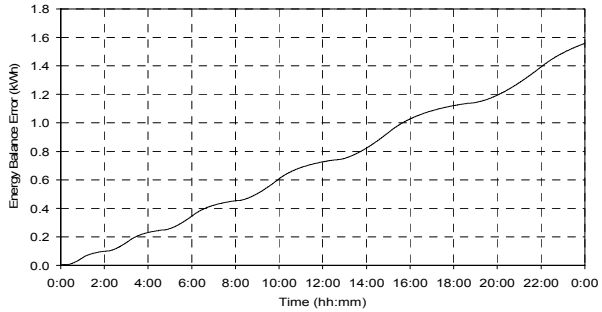

(g)

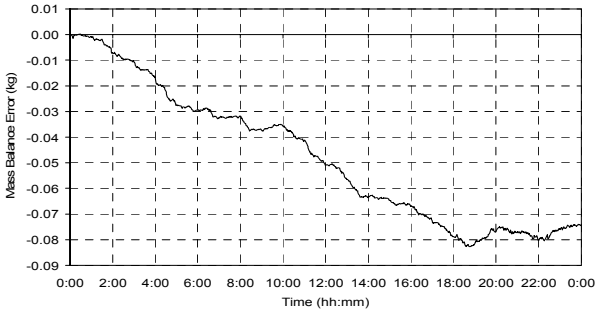

(h)

Figure 83 – Experiment 6.24 results.

6.3.25 Experiment 6.25

INITIAL STEADY STATE HEAT FLOW	INITIAL FREEZE LINING THICKNESS	INITIAL FREEZE LINING COMPOSITION	ELECTRICAL POWER HEAT FLOW	HEAT LOSSES HEAT FLOW	NET INPUT HEAT FLOW
250 kW	0.102 m	Rutile	1000 kW	0 kW	1000 kW

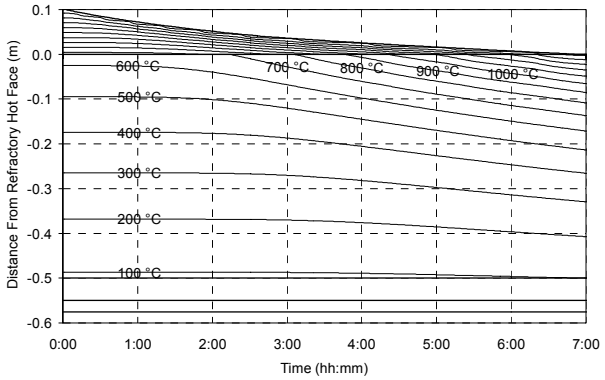

(a)

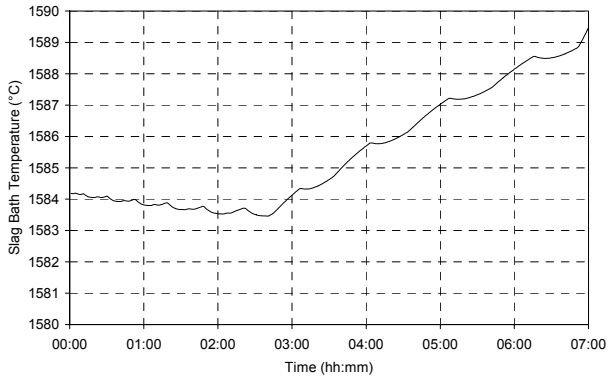

(b)

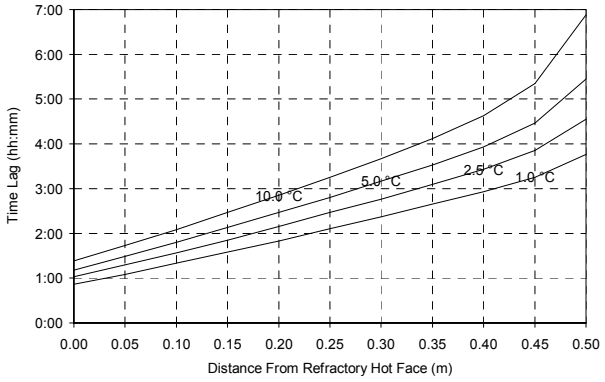

(c)

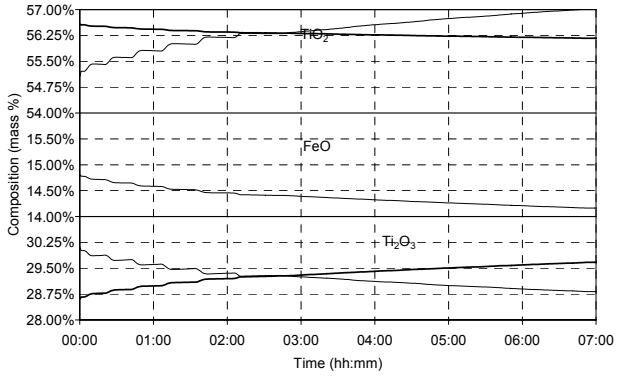

(d)

Not Plotted.

(e)

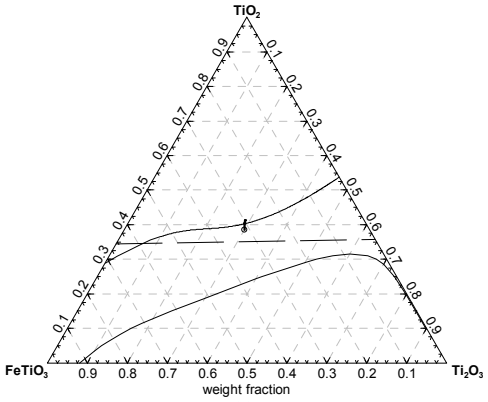

(f)

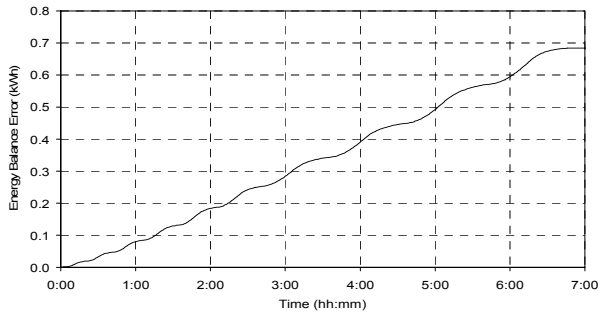

(g)

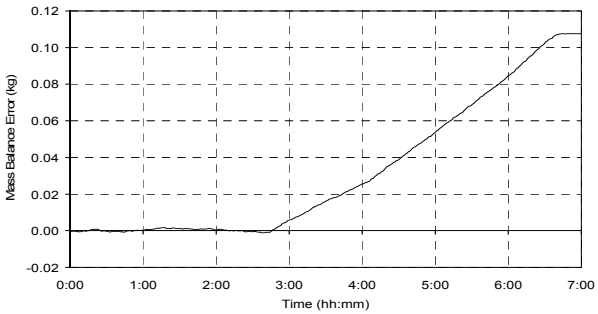

(h)

Figure 84 – Experiment 6.25 results.

6.3.26 Experiment 6.26

INITIAL STEADY STATE HEAT FLOW	INITIAL FREEZE LINING THICKNESS	INITIAL FREEZE LINING COMPOSITION	ELECTRICAL POWER HEAT FLOW	HEAT LOSSES HEAT FLOW	NET INPUT HEAT FLOW
250 kW	0.102 m	Rutile	10000 kW	0 kW	10000 kW

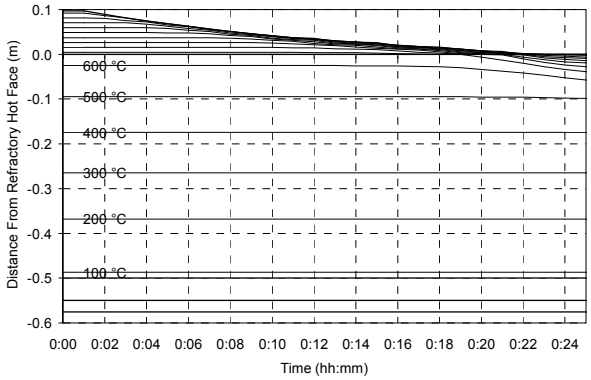

(a)

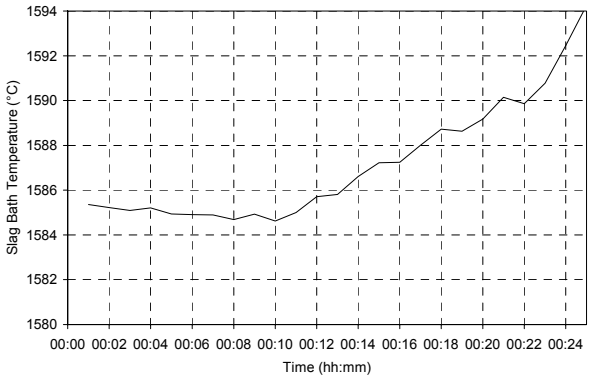

(b)

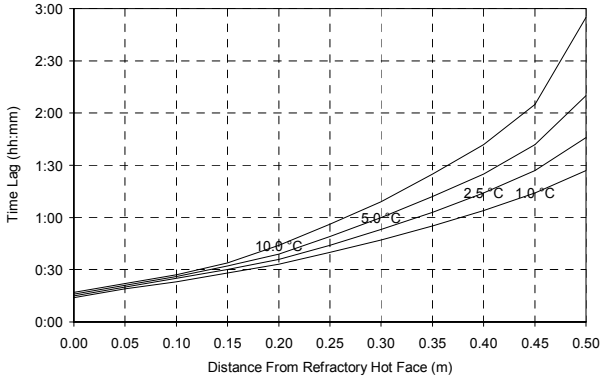

(c)

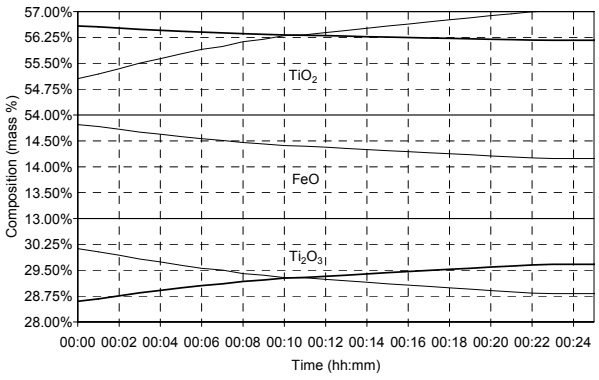

(d)

Not Plotted.

(e)

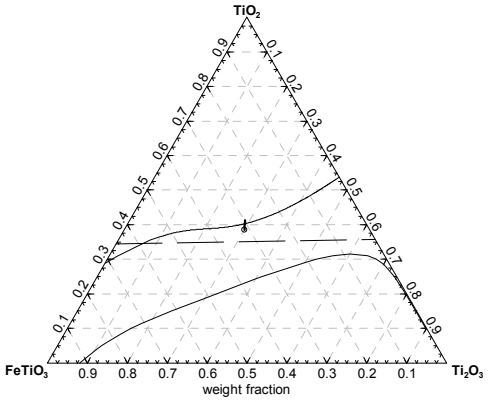

(f)

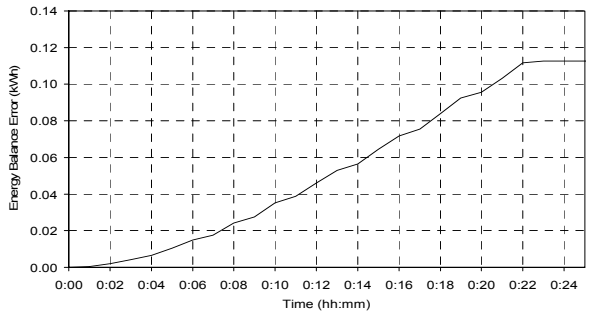

(g)

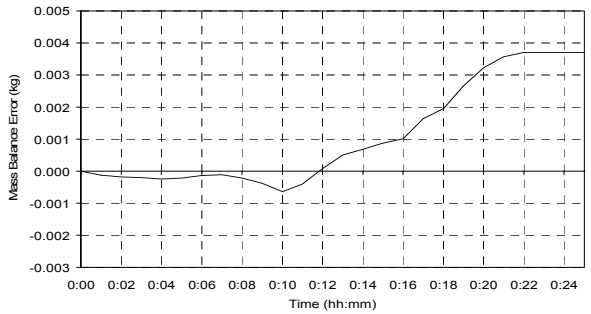

(h)

Figure 85 – Experiment 6.26 results.

6.4 DISCUSSION

6.4.1 Freeze Lining Thickness

From the experimental results the expected relationship between freeze lining thickness and net input heat flow rate is evident. A net input heat flow rate less than the initial steady state heat flow rate through the freeze lining and wall causes the freeze lining to become thicker. Conversely the freeze lining becomes thinner when the net input heat flow rate is greater than the initial steady state heat flow rate. This relationship is shown in Figure 86.

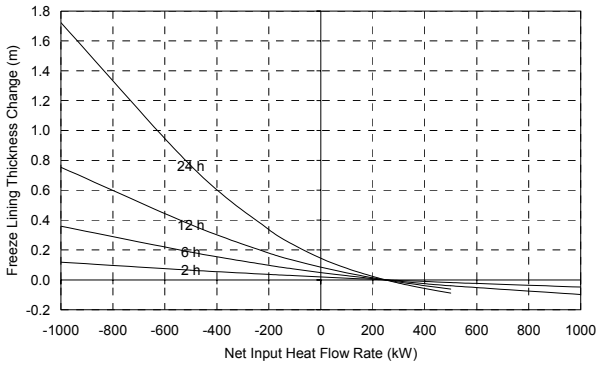

Figure 86 – Change in freeze lining thickness as a function of net input heat flow rate.

The chart was constructed with results from experiments 6.1 to 6.14. The initial freeze lining thickness for these experiments was 0.102 m.

When a net input heat flow rate of −1000 kW was applied, the freeze lining reached a thickness of around 1.8 m after 24 hours. It is unlikely that this will happen in reality. The experiments were set up to only allow solidification at the freeze lining hot face. In the actual process solidification will also occur on the slag bath surface, forming a crust. Such crust formation will tend, in time, to thermally insulate the slag bath and reduce the heat losses from the slag bath. This will result in slower increase in freeze lining thickness.

The results of those experiments with high net input heat flow rates (6.11, 6.12, 6.13, 6.14, 6.19, 6.20, 6.25 and 6.26) clearly show the damage that too high energy input rates can do to the freeze lining. Given that smelting furnaces in practice are equipped with power supplies with capacities between 20 MW and 40 MW, it is possible to melt away an entire freeze lining in a matter of minutes.

6.4.2 Thermal Response of Freeze Lining and Furnace Wall

From graph (a) in the experimental results the first observation is that the largest fall in temperature between the freeze lining hot face and the outer surface of the steel shell occurs in the freeze lining. This clearly demonstrates that the freeze lining represents the largest thermal resistance in the heat transfer circuit. The temperature falls by about 900 °C in the freeze lining in many instances.

A consequence of the large thermal resistance of the freeze lining is a slow thermal response in the brick layer of the furnace wall. The time lags at various positions in the wall are shown in graph (c). All the graph (c) results of experiments 6.1 to 6.14 are summarised in Figure 87 below. The graphs in Figure 87 show an asymptotic approach to the initial steady state heat flow rate (250 kW) from net input heat flow rate values less than and greater than the initial steady state value. This makes sense, since a net input heat flow rate equal to the initial steady state value will take an infinite period of time to register any temperature change at any position in the brick layer of the wall.

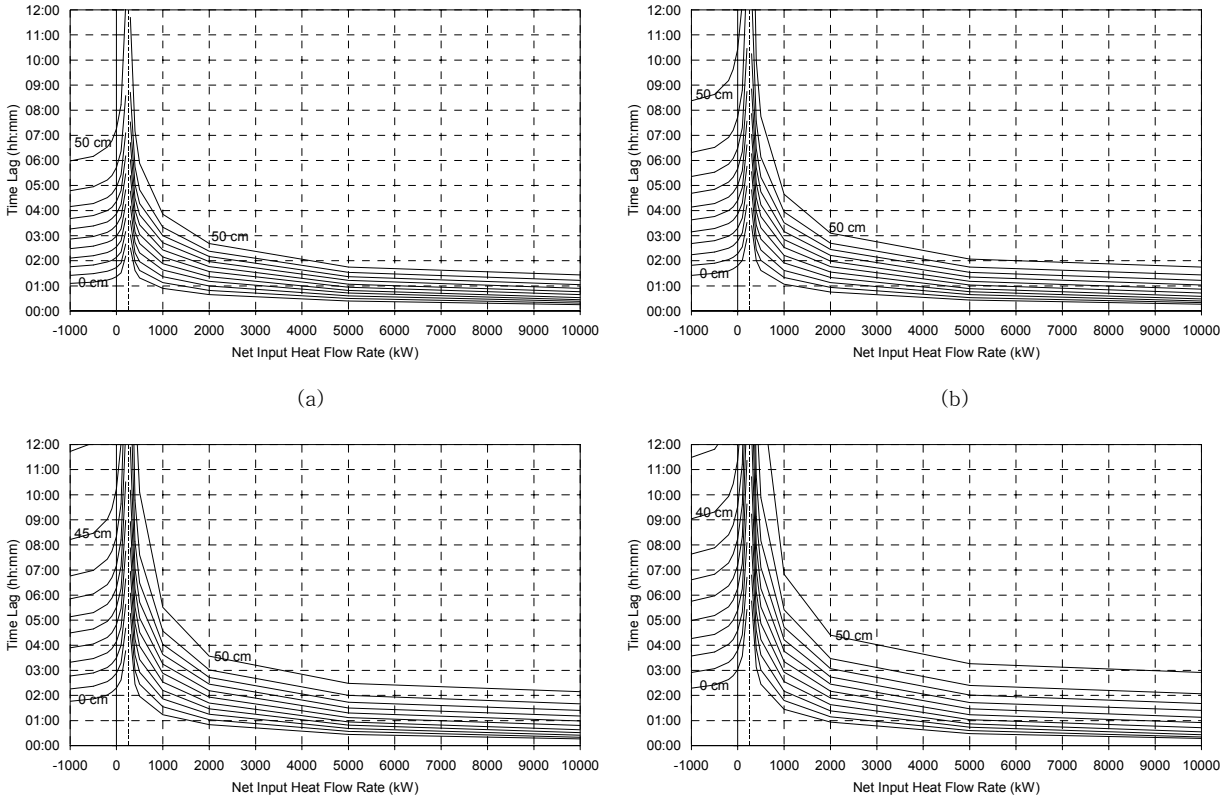

Figure 87 – Influence of net input heat flow rate on time lag in thermal response inside the brick wall.

The different curves on each graph represent different positions from the refractory hot face at 5 cm increments. The bottom curve represents a position on the refractory hot face. Chart (a) shows the time lag in detecting a 1.0 °C temperature change, (b) a 2.5 °C change, (c) a 5.0 °C change and (d) a 10.0 °C change. Data was taken from the results of experiments 6.1 to 6.14.

Also of interest is the lack of symmetry around the initial steady state heat flow rate value. In cases where the freeze lining thickness increased, temperatures in the brick layer were slower to respond compared with cases where the freeze lining thickness decreased. One can also conclude that temperatures in the brick layer take longer to fall than to rise. This is important to know when one is considering control of a freeze lining. The asymmetry in thermal response can be explained by considering the influence of solidification and melting on heat transfer in the freeze lining layer.

Figure 88 shows the temperature profile in the freeze lining layer 1 hour after changing the net input heat flow rate from the initial steady state value of 250 kW. For the −1000 kW case the difference in net input heat flow rate compared with the initial value is −1250 kW. For the 1000 and 2000 kW cases it is 750 kW and 1750 kW respectively. From this chart it is again clear that the melting cases have resulted in quicker thermal response inside the freeze lining than did the solidifying case. This, in turn, results in quicker thermal response in the brick layer of the furnace wall.

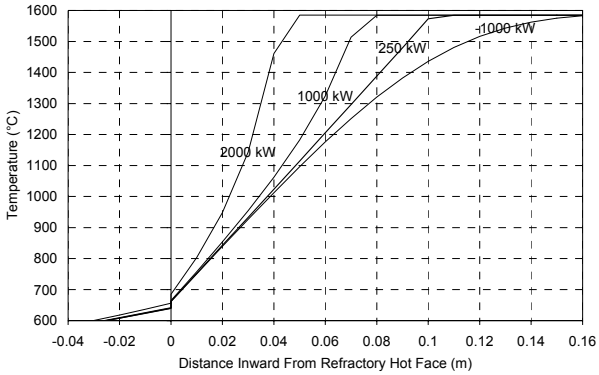

Figure 88 – Temperature profile in the freeze lining after 1 hour.

Cases shown include both solidification and melting.

Melting causes a reduction in freeze lining thickness and a reduction in the heat transfer resistance associated with the freeze lining. Heat therefore flows through the freeze lining and into the brick layer at a higher rate. This higher heat flow rate raises temperatures in the freeze lining and brick layer and yields a thermal response.

Solidification increases freeze lining thickness and the associated heat transfer resistance. In this case the rate at which heat is transferred into the freeze lining is reduced. For the brick layer to respond, the new lower heat flow rate must be propagated through the freeze lining and through the brick layer.

An increase in temperature is therefore dependent on conduction from the freeze lining hot face to the point in the brick layer where the temperature is monitored. This is because heat only needs to flow from the freeze lining hot face to the point of measurement to change the temperature at this point. In contrast, a decrease in temperature is dependent on conduction from the freeze lining hot face to the outside surface of the steel shell. The reason is that a reduction in temperature at the point of measurement needs heat to be removed from the outside surface of the steel shell. The heat transfer path is therefore generally shorter when detecting melting than when detecting solidification. This causes the asymmetric behaviour described above.

6.4.3 Slag Bath Composition

They 'wavy' profile of many of the graphs is the result of transitions from one finite difference node to the next.

The slag bath's composition was influenced in three ways during the experiments:

1. When the freeze lining grew thicker the slag bath TiO_2 and FeO content increased, and Ti_2O_3 content decreased.

   This observation can be made from the (d) graph of experiments 6.1 to 6.7, 6.15 to 6.17 and 6.21 to 6.23. It is also evident from the (f) graph of these experiments where such a graph was included, although it is slightly more difficult to detect due to the choice of axes (TiO_2–$FeTiO_3$–Ti_2O_3 rather than TiO_2–FeO–Ti_2O_3).

   This effect is simply the result of the phase chemistry of the slag. The composition of the slag that initially solidifies from the liquid is approximately 38%–62% ($FeTi_2O_5$–Ti_3O_5 by mass). This translates to a composition of approximately 12%–48%–40% (FeO–TiO_2–Ti_2O_3 by mass). Since the initial liquid slag composition is 15%–55%–30% (FeO–TiO_2–Ti_2O_3 by mass), the observed change in liquid slag composition is easily understood.

2. In the case of experiments 6.1 to 6.20, when the freeze lining was melted away the slag bath TiO_2 and FeO content decreased, and Ti_2O_3 content increased.

   This can be seen on the (d) graph of experiments 6.8 to 6.14 and 6.18 to 6.20.

   For these experiments the initial composition of the freeze lining was approximately 38%–62% ($FeTi_2O_5$–Ti_3O_5 by mass), or 12%–48%–40% (FeO–TiO_2–Ti_2O_3 by mass). Adding such material to liquid slag with composition 15%–55%–30% (FeO–TiO_2–Ti_2O_3 by mass) once again must yield the observed influence on liquid slag composition.

3. In the case of experiments 6.21 to 6.26, when the freeze lining was melted away the slag bath TiO_2 content increased, and the FeO and Ti_2O_3 content decreased.

   This is evident on the (d) and (f) graphs of experiments 6.24 to 6.26.

   Here the effect can again be explained based on a simple mass balance. Because the freeze lining used in these experiments initially consisted of pure TiO_2, melting this material into the bath can only result in an increase of liquid slag TiO_2 content.

Another observation of note is the convergence of liquid slag composition into the eutectic groove. This is entirely expected given the phase chemistry information presented in CHAPTER 2. The convergence into the eutectic groove is only observed for experiments in which a large degree of solidification took place. Such experiments include 6.1, 6.2, 6.15 and 6.21. From these experiments it is concluded that at least 0.7 m of additional freeze lining must solidify before the liquid slag composition reaches the eutectic groove.

The results of experiment 6.24 also show the liquid slag composition converging into the eutectic groove. This can however not be attributed to the same mechanism prevalent in experiments 6.1, 6.2, 6.15 and 6.21. In fact, the apparent convergence in the experiment 6.24 results occurred as a coincidence due to the choice of parameters used in the experiment. The results of experiments 6.25 and 6.26 shed some light on this matter. In both cases the liquid slag composition approaches the eutectic groove, but then crosses it. This is expected, since pure TiO_2 is being added from the freeze lining. Had experiment 6.24 therefore

been run for longer than 24 hours, its liquid slag composition would also have crossed over the eutectic groove.

6.4.4 Slag Bath Temperature

They 'wavy' profile of many of the temperature graphs is the result of transitions from one finite difference node to the next.

The observed changes in liquid slag composition discussed in the previous paragraph had a direct influence on liquid slag temperature. This is due to the model combining the slag bath with a portion of the freeze lining and bringing this combined mass of material to equilibrium. The end result of this procedure must be that the slag bath should follow closely the liquidus temperature of the slag. This is precisely what was observed. The same behaviour is expected in the actual process because of the inevitable interaction between slag bath and freeze lining.

For those experiments where the freeze lining became thicker, the liquid slag temperature dropped. This is consistent with the observed tendency of the liquid slag composition towards the eutectic groove. For those experiments where the freeze lining became thinner, the liquid slag temperature increased. This is because the material that is being absorbed from the freeze lining alters the slag bath composition in such a way that the slag's liquidus temperature becomes higher. If the initial freeze lining had consisted of pure ilmenite (This is of course a hypothetical possibility, given the low melting point of ilmenite.), the effect would have been reversed because adding pure ilmenite to the slag bath would lower its liquidus temperature. This is evident from the Figure 11 liquidus diagram.

There were some exceptions to the observed increase in liquid slag temperature with a decrease in freeze lining thickness. The results of experiments 6.24, 6.25 and 6.26 show the liquid slag temperature decreasing (at least initially) as the freeze lining becomes thinner. These experiments, specifically 6.25 and 6.26, are excellent examples of the liquid slag temperature following the slag's liquidus temperature.

Both these experiments show the liquid slag temperature decreasing until the slag composition reaches the eutectic groove. When the slag composition moves away from the eutectic groove, the liquid slag temperature starts to increase. This is expected, since the eutectic groove is after all a series of compositions where the slag liquidus temperature is lower than for compositions on either side of it.

6.4.5 Freeze Lining Composition

The variation of freeze lining composition with time is shown in graph (e) for those experiments where the freeze lining became thicker (6.1 to 6.7, 6.15 to 6.17 and 6.21 to 6.23). Because a relatively small amount of slag solidified during most of these experiments, the composition of slag that solidified at the freeze lining hot face remained mostly constant.

Significant changes in solid slag composition were only observed for experiments 6.1, 6.2, 6.15 and 6.21. During these experiments the liquid slag composition reached the eutectic groove, which resulted in slag solidification producing rutile in addition to the pseudobrookite phase that was always present. A change in the composition of the pseudobrookite phase is also evident before the point where rutile becomes stable.

The pseudobrookite phase tended to become richer in the $FeTi_2O_5$ end member as solidification progressed. This is expected, since the liquid slag phase became richer in FeO and TiO_2 with time.